QUANTUM UNCERTAINTY AND CONSERVATION LAW RESTRICTIONS ON GATE FIDELITY

by

Nathan John Steiger

Submitted to Brigham Young University in partial fulfillment

of graduation requirements for University Honors

Department of Physics and Astronomy

May 2010

Advisor: Jean-François S. Van Huele Honors Representative: Steve Turley

Signature: _____ Signature: _____

BRIGHAM YOUNG UNIVERSITY

DEPARTMENT APPROVAL

of a senior thesis submitted by

Nathan John Steiger

This thesis has been reviewed by the research advisor, research coordinator, and department chair and has been found to be satisfactory.

Date	Jean-François S. Van Huele, Advisor
Date	Eric Hintz, Research Coordinator
Date	Ross L. Spencer, Chair

ABSTRACT

QUANTUM UNCERTAINTY AND CONSERVATION LAW RESTRICTIONS ON GATE FIDELITY

Nathan John Steiger

Department of Physics and Astronomy

Bachelor of Science

This work explores several formulations of inherent limitations in quantum theory. Ever since its inception with Heisenberg in 1927, uncertainty has played the lead role in imposing such limitations [1]. Yet the ubiquitous Heisenberg uncertainty principle, $\Delta x \Delta p \approx h$, and its generalized version developed by Robertson [2] can be strengthened in many cases. I discuss and present a new derivation of a physically and mathematically extended uncertainty relation for both pure and mixed states that Schrödinger originally developed [3]. I illustrate the discrepancies between the Robertson and Schrödinger uncertainty relations by applying them to a selection of incompatible operators. I work out these uncertainties in one dimension for the infinite square well, the harmonic oscillator, and the free particle wave packet; I also expand upon my previous work [4] to calculate uncertainties for operators and states in the space of angular momentum 1/2, 1, 3/2, and 2. Incorporating the Schrödinger

uncertainty relation often raises the lower bound on uncertainty with respect to incorporating the Robertson uncertainty relation.

Furthermore, I connect the Schrödinger form of uncertainty to conservation law constraints and analyze some limitations on quantum computational processes. Recent work by Karasawa et al. [5] suggests that conservation laws limit the inherent accuracy of gate operations in quantum computing. One way to quantify these limitations is through a gate operation's fidelity. I extend and clarify this work on arbitrary single-qubit gate operations by incorporating the Schrödinger form of the uncertainty relation. From this, I propose an approximate computational feasibility check that suggests an upper bound on fidelity for certain quantum computations.

ACKNOWLEDGMENTS

I express my sincerest thanks to Dr. Jean-François Van Huele, without whom this work would have been impossible. I gratefully acknowledge the many hours of assistance and guidance that he has generously given me for over two years.

I am also indebted to Dr. Peter Pemberton-Ross of the Department of Applied Mathematics and Theoretical Physics at Cambridge University for his help, guidance, and encouragement.

Contents

Table of Contents vii

List of Figures ix

1 Introduction 1
- 1.1 Quantum Uncertainty . . . 1
- 1.2 Spin Systems . . . 4
  - 1.2.1 Classical and Quantum Spin . . . 4
  - 1.2.2 Quantum Angular Momentum Operators . . . 6
  - 1.2.3 Quantum States . . . 7
- 1.3 Quantum Computing . . . 7
  - 1.3.1 Limitations . . . 8
  - 1.3.2 Qubit States . . . 9
  - 1.3.3 Thesis Overview . . . 10

2 Uncertainty Derivations 13
- 2.1 Heisenberg and Robertson Uncertainty Relations . . . 13
- 2.2 Schrödinger Uncertainty Relation . . . 14
- 2.3 Uncertainty for Mixed States . . . 17
  - 2.3.1 Mixed States, the Density Operator, and Uncertainty . . . 17
  - 2.3.2 Schrödinger Uncertainty Relation For Mixed States . . . 19
- 2.4 Discussion of Uncertainty and Uncertainty Relations . . . 22

3 Uncertainty Data 25
- 3.1 Uncertainty in One Dimension . . . 25
  - 3.1.1 The Infinite Square Well . . . 26
  - 3.1.2 The Harmonic Oscillator . . . 27
  - 3.1.3 The Free-Particle Wave Packet . . . 27
- 3.2 Discussion of One-Dimensional Data . . . 30
- 3.3 Uncertainty for Angular Momentum . . . 30
  - 3.3.1 Spin-1/2 Uncertainty . . . 31
  - 3.3.2 Angular Momentum Uncertainty . . . 33
  - 3.3.3 Spin Mixed State Uncertainty . . . 35

3.4 Discussion of Angular Momentum Data 38

4 Fidelity Analysis **41**
4.1 Quantum Gate Fidelity Derivation 41
4.1.1 Quantum Gates 41
4.1.2 Gate Fidelity 43
4.2 Conservation Laws and Gate Fidelity 44
4.3 Fidelity Employing the Schrödinger Uncertainty Relation 46

5 Fidelity Data **49**
5.1 Calculating Fidelity 49
5.2 Fidelity in Three Specific Cases 52
5.3 Discussion of Fidelity Data 57

6 Conclusions **59**

A Angular Momentum Matrices **61**

B *Mathematica* Code for Numerical Spin Eigenvalues and Eigenvectors **63**
B.1 Code for $\mathbf{J}_r^{(1)}$ 63
B.2 Code for $\mathbf{J}_r^{(3/2)}$ 66
B.3 Code for $\mathbf{J}_r^{(2)}$ 69

C *Mathematica* Code for Numerical Calculations of Fidelity via Operator Norms **73**

Index **75**

Bibliography **76**

List of Figures

1.1 Angular and Spin Momentum 5
1.2 Quantum State Representation in Spherical Coordinates 7
1.3 Astronaut Decoherence and Fidelity 8
1.4 Bloch Sphere and Quantum States 10

3.1 Harmonic Oscillator Levels and States 27
3.2 Gaussian and Non-Gaussian Wavepackets 29
3.3 Representation and Use of General Quantum States 32
3.4 Uncertainties for Spin Operators 34
3.5 Uncertainties for Combinations of Spin Operators 34
3.6 Mixed State Spin Operator Standard Deviations 36
3.7 Mixed State Spin Operator Robertson Uncertainty 36
3.8 Mixed State Spin Operator Schrödinger Uncertainty 36
3.9 Uncertainty for Orbital Angular Momentum 39

4.1 Hadamard Gate Visualization 43

5.1 Numerical Gate Fidelity 54
5.2 Bloch Sphere Gate Fidelity 56

List of Tables

1.1 Progression of Uncertainty Relations 3

3.1 Infinite Square Well Uncertainty 26
3.2 Harmonic Oscillator Uncertainty 28
3.3 Gaussian Free-Particle Wave Packet Uncertainty 29
3.4 Non-Gaussian Free-Particle Wave Packet Uncertainty 29
3.5 Angular Momentum Uncertainty 37

5.1 Numerical Fidelity Data 55

Chapter 1

Introduction

1.1 Quantum Uncertainty

Quantum uncertainty forms the crux of this thesis. A precise application of quantum mechanics must invariably confront the limitations imposed by uncertainty. An understanding of the nature of those limitations is thus imperative. Indeed, quantum mechanics has come to be characterized—at least in its popularized version—by the iconic and controversial assertion of Werner Heisenberg that "It seems to be a general law of nature that we cannot determine position and velocity simultaneously with arbitrary accuracy" [6, 7]. This was the first profound insight into the quantum characteristics of nature: that certain pairs of observables cannot be measured both accurately and simultaneously.

The debate over the significance of this uncertainty restriction, begun by Albert Einstein and Niels Bohr in the 1920s, continues today [8]. After over 80 years of research and overwhelming experimental evidence, this fundamental assumption of quantum mechanics that certain observables are fundamentally incompatible seems inescapable. This has led some [9] to assert with Stephen Hawking that "Even God

is bound by the uncertainty principle and cannot know both the position and momentum" [10].

Heisenberg originally thought of uncertainty in an intuitive way. He pictured a microscope through which one could view very small objects. Heisenberg proposed a *Gedankenexperiment* in which one uses high-frequency photons to improve the resolution of what is being imaged. In his seminal paper on uncertainty [6, 7] Heisenberg explains, "Let one illuminate the electron and observe it under a microscope. Then the highest attainable accuracy in the measurement of position is governed by the wavelength of the light. However, in principle one can build, say, a gamma-ray microscope and with it carry out the determination of position with as much accuracy as one wants." However, he notes, since gamma rays have high-frequency and energy, they will greatly disturb the electron being observed. The observed electron undergoes "a discontinuous change of momentum." Essentially, it is a Catch-22; the high-frequency gamma ray determines the position very accurately, yet it disturbs the electron so much that one looses track of the momentum. Likewise, if one uses lower frequency photons, such as microwaves, the momentum will be much more certain, but the position will become fuzzy. All of this is encapsulated in his uncertainty principle

$$\Delta\hat{x}\Delta\hat{p} \approx h\,, \tag{1.1}$$

where $\Delta\hat{x}$ is the uncertainty of knowledge about the position of the particle, $\Delta\hat{p}$ is the uncertainty associated with the momentum of the particle, and h is Planck's constant.[1]

Since the time of Heisenberg, the uncertainty relation has become increasingly

[1]Max Planck had introduced $h = 6.626 \times 10^{-34}$J·s to describe the smallest possible amount of "action" (energy multiplied by time) involved in quantum processes [11] and Heisenberg used this as his lower bound.

Table 1.1 The progression of uncertainty relations. I give the names of the people who developed each equation along with the year they published their work in parentheses. The arrow denoted by $\Longrightarrow$ indicates a progression forward; each step in the process, from Heisenberg to Weyl to Robertson to Schrödinger, expands the uncertainty principle further.

Heisenberg (1927)	Weyl (1928)
$\Delta x \Delta p \approx h$	$\sigma_x \sigma_p \geq \frac{\hbar}{2}$
Robertson (1929)	Schrödinger (1930)
$\sigma_A \sigma_B \geq \frac{1}{2i}\langle[\hat{A}, \hat{B}]\rangle$	$\sigma_A \sigma_B \geq \sqrt{\left(\frac{1}{2}\langle\{\hat{A}, \hat{B}\}\rangle - \langle\hat{A}\rangle\langle\hat{B}\rangle\right)^2 + \left(\frac{1}{2i}\langle[\hat{A}, \hat{B}]\rangle\right)^2}$

nuanced; our understanding of it has undergone both a qualitative and a quantitative change. On the qualitative side, uncertainty is seen to have a broader scope than the limited version of Heisenberg's *Gedankenexperiment*; it is seen in terms of the multifaceted process of quantum measurement. On the quantitative side, Heisenberg's uncertainty principle has been translated into the more formal language of quantum mechanics and given various interpretations and reformulations.

This thesis will highlight some important transitions and the attributes of the uncertainty relations. The uncertainty relation has undergone different transitions, with each transition producing a more complete uncertainty relation. The progression from Heisenberg [6], to Weyl [12], to Robertson [2], and to Schrödinger [3] can been seen diagrammatically in Table 1.1. I focus on this four-step progression in this thesis because these four forms of the uncertainty relation are the most commonly used, and they form the basis from which others have been developed; uncertainty and uncertainty relations are a broad topic, and there are books entirely devoted to the subject (see [13, 14]), so this thesis will highlight only key points.

I primarily use the Robertson and Schrödinger uncertainty relations (see Table 1.1) in this thesis by calculating the standard deviations and expectation values for various operators and states. In my results, I find a range of outcomes: sometimes the Robertson and Schrödinger relations give the same answer, sometimes the Robertson relation predicts no uncertainty while the Schrödinger picks up uncertainty, and sometimes the Schrödinger relation expands the uncertainty found by the Robertson relation.

1.2 Spin Systems

In this thesis, I employ quantum mechanical spin to further illustrate the differences between the Robertson and Schrödinger uncertainty relations and also to highlight the nature of conservation law constraints in quantum computational processes. Spin plays a primary role because of its relative simplicity, its usefulness in illustrating quantum mechanical ideas, and its wide range of applications. Consequently, I will give an overview of how spin is defined and briefly discuss some of the key elements of spin that I utilized.

1.2.1 Classical and Quantum Spin

In classical mechanics (as opposed to quantum mechanics), a rigid object can have two different types of angular momentum: orbital and spin. Like the earth orbiting the sun, orbital angular momentum is associated with the approximately circular trajectory of the object; like the daily rotations of the earth or of a spinning top, spin angular momentum is associated with the motion of an object about the center of mass [9]. As exhibited in Fig. 1.1, a planet orbiting a star has a vector angular momentum $\boldsymbol{L} = \boldsymbol{r} \times \boldsymbol{p}$ (where $\boldsymbol{r}$ is the radial vector going from the star to the planet

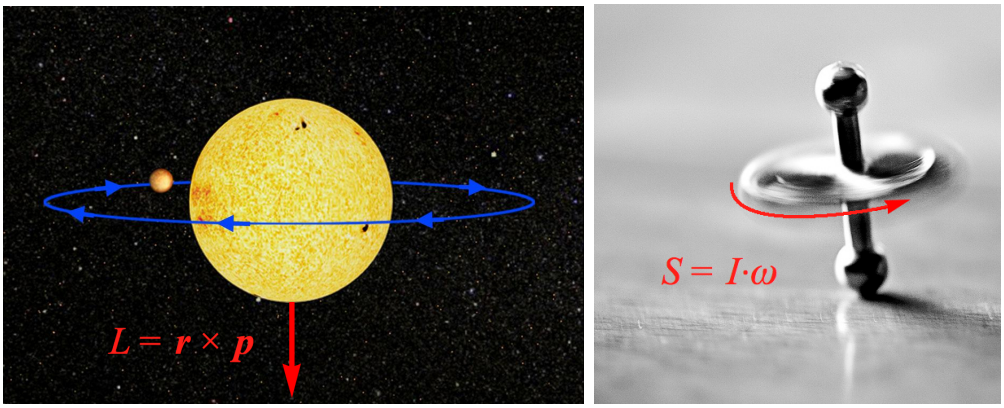

Figure 1.1 The system of a planet orbiting a star [15] has an angular momentum $\boldsymbol{L} = \boldsymbol{r} \times \boldsymbol{p}$ where $\boldsymbol{r}$ is the radius or distance between the planet and the star and where $\boldsymbol{p}$ is the momentum of the planet. A spinning top has physical "spin" which can be written as: $\boldsymbol{S} = \boldsymbol{I} \cdot \boldsymbol{\omega}$, where $\boldsymbol{I}$ is the moment of inertia tensor and $\boldsymbol{\omega}$ is the vector angular velocity of the top.

and where the vector quantity $\boldsymbol{p}$ is the momentum of the planet), and the spinning top has a vector spin momentum $\boldsymbol{S} = \boldsymbol{I} \cdot \boldsymbol{\omega}$ (where $\boldsymbol{I}$ is the moment of inertia tensor and $\boldsymbol{\omega}$ is the vector angular velocity of the top).

Although $\boldsymbol{L}$ and $\boldsymbol{S}$ are often separately identified, that separation is really just a matter of convenience; if one were to label all the particles that make up a spinning top and then calculate and sum all their orbital angular momenta about the center of mass, one would arrive at the value $\boldsymbol{S}$. By contrast, very small things like microscopic particles are quantum mechanical objects and must be treated differently. Spin in quantum mechanics is therefore fundamentally different from spin in classical mechanics: a particle's spin is *intrinsic* and does not directly coincide with an actual rotation of the particle. Though an electron may be represented as orbiting a nucleus and thus have an orbital angular momentum $\boldsymbol{L}$, the electron's spin $\boldsymbol{S}$ is inherent and immutable. As it turns out, every particle has an intrinsic spin value: electrons have spin 1/2; photons have spin 1; Δ baryons have spin 3/2; gravitons have spin 2; and so on.

1.2.2 Quantum Angular Momentum Operators

The classification "angular momentum" includes both spin and orbital angular momentum. The algebra of spin and orbital angular momentum—and thus quantum angular momentum in general—rely on the same principles. The entire theory of quantum angular momentum stems from the commutation rules

$$[J_i, J_j] = i\hbar\epsilon_{ijk}J_k\,, \tag{1.2}$$

where $[J_i, J_j] = J_iJ_j - J_jJ_i$, the constant $\hbar = h/2\pi$, $(i, j, k) = (1, 2, 3)$, ϵ_{ijk} is the Levi-Civita symbol, J_i stands for any angular momentum, and the Einstein summation convention is implied. From Eq. (1.2) one can derive orbital angular momentum states and spin states, the Pauli matrices, orbital angular momentum and spin operator representations, and much more. In this thesis I will focus particularly on orbital angular momentum and spin states and orbital angular momentum and spin operators because they illustrate uncertainty relations in a clear way.

Throughout the discussion on spin uncertainty and quantum computation, I utilize orbital angular momentum and spin operators. For spin 1/2, the operators are written as

$$S_i = \frac{\hbar}{2}\sigma_i \tag{1.3}$$

where $i = x, y, z$ and σ_i corresponds to the Pauli matrices

$$\sigma_x = \begin{pmatrix} 0 & 1 \\ 1 & 0 \end{pmatrix} \qquad \sigma_y = \begin{pmatrix} 0 & -i \\ i & 0 \end{pmatrix} \qquad \sigma_z = \begin{pmatrix} 1 & 0 \\ 0 & -1 \end{pmatrix} \quad . \tag{1.4}$$

The operators for higher values of spin, such as 1, 3/2, and 2, are similar.

1.2.3 Quantum States

States in quantum mechanics are critical for calculating expectation values and thus uncertainty equations. For spin and orbital angular momentum, I calculated expectation values using generalized states which are extensions of single states. Single states can be written as the sum of the basis vectors for that state; for example, a single state that happens to have three basis vectors can be written as

$$|\psi\rangle = a_1|\psi_1\rangle + a_2|\psi_2\rangle + a_3|\psi_3\rangle\,,$$

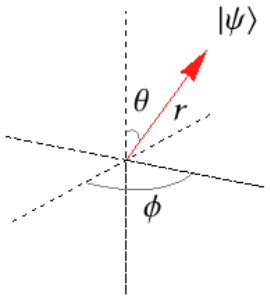

Figure 1.2 Any angular momentum quantum state $|\psi\rangle$ can be represented by a vector using the spherical coordinates (r, θ, ϕ) where r is the magnitude of the state. States are most often normalized, making $|r| = 1$.

where $|\psi_1\rangle$, $|\psi_2\rangle$, and $|\psi_3\rangle$ are the basis vectors and a_1, a_2, and a_3 are arbitrary complex coefficients. Generalized states differ from single states in that the components, such as a_1, a_2, and a_3 from above, are parameterized such that one can point the state in any direction by merely specifying two angles and a magnitude (see Fig. 1.2.2). For spin 1/2, which has two basis vectors, one of these generalized states can be written as

$$|\chi\rangle = \cos(\theta/2)|\psi_1\rangle + e^{i\phi}\sin(\theta/2)|\psi_2\rangle\,,$$

where one has only to specify the angles θ and ϕ and then one will know where the state is located. Chapter 3 contains a fuller discussion of generalized states and how I use them in the calculations.

1.3 Quantum Computing

Quantum information science has sought answers to the question: is there any advantage to be gained by storing, transmitting, and processing information encoded in quantum systems? After intense research spanning the past several decades the

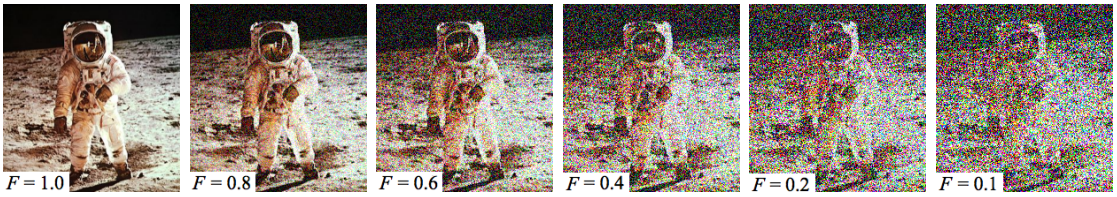

Figure 1.3 Astronaut decoherence and corresponding fidelity. This sequence of photographs of an astronaut is analogous to the decoherence of a quantum state. The quantum state starts out clear and with all the intended information, but over time or through the process of performing a calculation the state can decohere until it is not longer clearly distinguishable. Fidelity, F, which has the range $0 \leq F \leq 1$, can be used to characterize how well a quantum process is performing. Quantum computational processes that keep a state clear and free of noise, have high fidelity (near 1) whereas low fidelity processes make the state decohere too quickly.

consensus answer has developed into a resolute yes. Today, many research groups around the world work towards the ambitious technological goal of building a quantum computer [16]. This thesis focuses on understanding the limitations inherent in quantum computational processes essential for quantum computing. In this section I discuss the ideas behind limitations inherent in quantum computing (quantified by using the Schrödinger uncertainty relation) and how quantum computational states are represented—both crucial concepts in my thesis.

1.3.1 Limitations

Several factors limit the process of quantum computing. Any quantum computer must be sufficiently isolated from the world around it to prevent "decoherence." A state undergoing decoherence loses its inherent quantum properties; in a sense, the quantum state becomes fuzzy (see Fig. 1.3). A quantum state that decoheres too quickly loses its usefulness for quantum computing. Thus it is essential to understand the sources of decoherence and ways to avoid them.

Decoherence comes from several sources: the environment in which the quantum computer resides, controlling or handling the quantum state, and from conservation

law constraints. A large amount of literature exists that discusses how to correct for environmental and controller-induced decoherence [17, 18], yet there is little discussion of the limitations imposed by conservation laws. Chapters 4 and 5 focus on conservation law decoherence and limitations.

A valuable connection between uncertainty and quantum computing is fidelity. Fidelity is one of the primary measures of how well information in a state is preserved through a computation; fidelity, F, has the range $0 \leq F \leq 1$, where 1 indicates perfect fidelity and 0 indicates the lowest possible fidelity. I illustrate with an example: if a quantum computer takes an initial memory state $|\psi\rangle$ and performs some dynamical process, noise and decoherence will almost invariably be introduced into the state; if $|\psi\rangle$ has obtained little noise, then the fidelity will be high (see Fig. 1.3). Processes of high fidelity correspond to low uncertainty and the connection between the two will be discussed in Chapter 4.

1.3.2 Qubit States

Two-level states, such as $|\psi\rangle = a_0|0\rangle + a_1|1\rangle$ known as qubits, are particularly useful for quantum information because they hold the 0's and 1's that are so essential for computation. Current computers encode information into 0's and 1's and then perform the calculations based on large strings of these numbers. For example, the binary equivalent of the words "Physics is cool" is encoded as: 01010000 01101000 01111001 01110011 01101001 01100011 01110011 00100000 01101001 01110011 00100000 01100011 01101111 01101111 01101100 00001101 00001010. Quantum computers similarly need to transform information into two-valued pieces of data; the basic building block is often the state $|\psi\rangle = a_0|0\rangle + a_1|1\rangle$ which can, for example, represent the possibility of an electron being in the spot designated by $|0\rangle$ or in the spot designated by $|1\rangle$.

Two-level states can also be represented on the Bloch sphere. The Bloch sphere

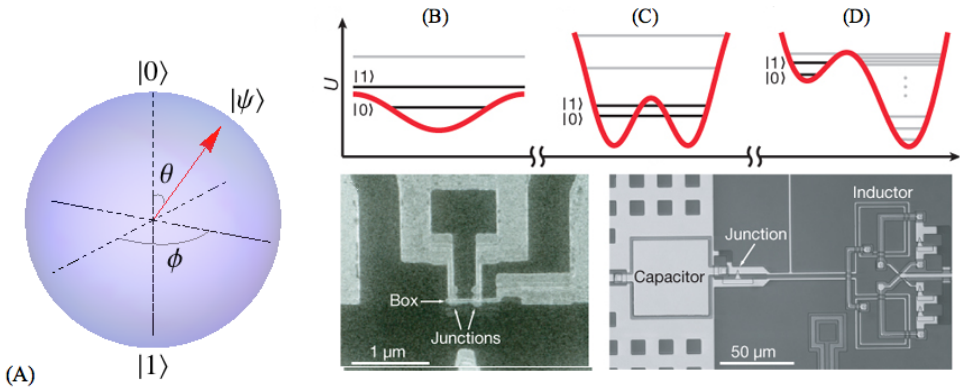

Figure 1.4 (A) The Bloch sphere is a special case of spherical coordinates; states that live on the Bloch sphere all have a magnitude of 1 (which is on the surface of the sphere), they can be designated by two angles (θ, ϕ), and they have two basis states, typically chosen to be $|0\rangle$ and $|1\rangle$. The Bloch sphere is often used to represent or visualize a two-level state. (B)-(D) The plots give potential wells where two levels are utilized to store information ($|0\rangle$ and $|1\rangle$) and below these are shown two experimental realizations of these potential wells [16].

is a unit sphere (a sphere of radius 1) and states can be represented as a point on the surface of the sphere or a vector directed to that point (see Fig. 1.4(A)). I will often use the Bloch sphere when discussing quantum computing and presenting some my calculations (Chapters 4 and 5).

1.3.3 Thesis Overview

In Chapter 2 I discuss various forms of the uncertainty relation. I then give new derivations of the Schrödinger uncertainty relation for both pure and mixed states. In Chapter 3 I compare and contrast the Robertson and Schrödinger uncertainty relations by showing the results of calculations for various quantum operators and states. In Chapter 4 I show how the Schrödinger uncertainty relation places constraints on the fidelity of single-qubit quantum gates. In Chapter 5 I compare and contrast the use of the Robertson and Schrödinger uncertainty relations for the fidelity of three different situations. In Chapter 6 I conclude that incorporating conservation law con-

straints and the Schrödinger uncertainty relation may impose important limitations on quantum gate fidelity.

In this thesis I define the terms and equations that I use to the best of my ability, but I do not have the space nor the time to fully explain every principle and equation. This thesis is based on the principles of quantum mechanics and quantum computation and if the reader is unfamiliar with certain principles or equations, I invite the reader to consult some of the excellent texts on quantum mechanics (such as [9, 19]) and quantum computation (such as [18]).

Chapter 2

Uncertainty Derivations

2.1 Heisenberg and Robertson Uncertainty Relations

There have been several improvements on the Heisenberg uncertainty principle, Eq. (1.1). A year after Heisenberg formulated Eq. (1.1), Weyl derived [12] the more formal relation

$$\sigma_x \sigma_p \geq \frac{\hbar}{2}\,, \tag{2.1}$$

where σ_x and σ_p are standard deviations of the two operators $\hat{x}$ and $\hat{p}$ defined for an arbitrary Hermitian operator $\hat{\mathcal{O}}$ as $\sigma_{\mathcal{O}} = \sqrt{\langle \hat{\mathcal{O}}^2 \rangle - \langle \hat{\mathcal{O}} \rangle^2}$. Going even further, Robertson [2] generalized Eq. (2.1) for arbitrary Hermitian operators $\hat{A}$ and $\hat{B}$

$$\sigma_A \sigma_B \geq \frac{1}{2i} \langle [\hat{A}, \hat{B}] \rangle\,, \tag{2.2}$$

where σ_A and σ_B are the standard deviations and where $[\hat{A}, \hat{B}]$ represents the commutator $[\hat{A}, \hat{B}] \equiv \hat{A}\hat{B} - \hat{B}\hat{A}$ or the incompatibility of the two operators $\hat{A}$ and $\hat{B}$. The majority of quantum textbooks—and consequently many research papers which use uncertainty—get only as far as the Robertson relation. One of the purposes of

this work is to show the limitations and some of the pitfalls of using the Robertson uncertainty relation.

2.2 Schrödinger Uncertainty Relation

Though Heisenberg's uncertainty principle and Robertson's version of the uncertainty relation are part of the foundation of quantum mechanics, other versions of the uncertainty relation—including the Schrödinger uncertainty relation—have received comparatively little attention in the physics literature. The Schrödinger uncertainty relation was initially published in an inconspicuous German journal [3] that periodically reported on the activity of the Prussian Academy [20]. I believe that these factors have led to the cursory coverage the Schrödinger uncertainty relation receives in the literature.

Schrödinger derived the following uncertainty relation

$$\sigma_A \sigma_B \geq \sqrt{\Big(\frac{1}{2}\langle\{\hat{A},\hat{B}\}\rangle - \langle\hat{A}\rangle\langle\hat{B}\rangle\Big)^2 + \Big(\frac{1}{2i}\langle[\hat{A},\hat{B}]\rangle\Big)^2}. \tag{2.3}$$

The difference between Eqs. (2.2) and (2.3) is the first squared term under the square root, known in a classical statistics sense as the covariance, consisting of the anti-commutator $\{\hat{A},\hat{B}\}$, defined as $\{\hat{A},\hat{B}\} \equiv \hat{A}\hat{B} + \hat{B}\hat{A}$, and the product of two expectation values $\langle\hat{A}\rangle\langle\hat{B}\rangle$. These extra terms lead to substantial differences between the two uncertainty relations Eqs. (2.2) and (2.3) in many cases. In this thesis I will show how salient these differences can be. From this point onward, I will frequently call the right hand sides of Eqs. (2.2) and (2.3) the Robertson and Schrödinger uncertainties respectively.

I now derive the Schrödinger uncertainty relation. The derivation shown here incorporates and builds off of those done in Robertson [2], Schrödinger [3] and Griffiths [9]. For any Hermitian operator $\hat{A}$, based upon the standard deviation definition, I

have

$$\sigma_A^2 = \langle(\hat{A} - \langle\hat{A}\rangle)\Psi|(\hat{A} - \langle\hat{A}\rangle)\Psi\rangle.$$

I let $|f\rangle = |(\hat{A} - \langle\hat{A}\rangle)\Psi\rangle$ and thus

$$\sigma_A^2 = \langle f|f\rangle\,.$$

Similarly, for any other Hermitian operator $\hat{B}$ in the same state

$$\sigma_B^2 = \langle(\hat{B} - \langle\hat{B}\rangle)\Psi|(\hat{B} - \langle\hat{B}\rangle)\Psi\rangle = \langle g|g\rangle$$

for $|g\rangle = |(\hat{B} - \langle\hat{B}\rangle)\Psi\rangle$. The product of the two deviations can thus be expressed as

$$\sigma_A^2\sigma_B^2 = \langle f|f\rangle\langle g|g\rangle\,. \tag{2.4}$$

In order to relate the two vectors $|f\rangle$ and $|g\rangle$, I use the Schwarz inequality (see [21] pg. 246) which is defined as

$$\langle f|f\rangle\langle g|g\rangle \geq |\langle f|g\rangle|^2\,, \tag{2.5}$$

and thus Eq. (2.4) can be written as

$$\sigma_A^2\sigma_B^2 \geq |\langle f|g\rangle|^2\,. \tag{2.6}$$

Since $\langle f|g\rangle$ is in general a complex number, I use the fact that the modulus squared of any complex number z is defined as

$$|z|^2 = zz^*,$$

where z^* is the complex conjugate of z. The modulus squared can also be expressed as

$$|z|^2 = \Big(\mathrm{Re}(z)\Big)^2 + \Big(\mathrm{Im}(z)\Big)^2 = \Big(\frac{z+z^*}{2}\Big)^2 + \Big(\frac{z-z^*}{2i}\Big)^2. \tag{2.7}$$

I let $z = \langle f|g\rangle$ and $z^* = \langle g|f\rangle$ and substitue these into Eq. (2.7) to get

$$|\langle f|g\rangle|^2 = \left(\frac{\langle f|g\rangle + \langle g|f\rangle}{2}\right)^2 + \left(\frac{\langle f|g\rangle - \langle g|f\rangle}{2i}\right)^2. \tag{2.8}$$

The inner product $\langle f|g\rangle$ is written out explicitly as

$$\langle f|g\rangle = \langle \Psi(\hat{A} - \langle\hat{A}\rangle)|(\hat{B} - \langle\hat{B}\rangle)\Psi\rangle,$$

and using the fact that $\hat{A}$ and $\hat{B}$ are Hermitian operators, I find

$$\begin{aligned}
\langle f|g\rangle &= \langle \Psi|(\hat{A} - \langle\hat{A}\rangle)(\hat{B} - \langle\hat{B}\rangle)\Psi\rangle \\
&= \langle \Psi|(\hat{A}\hat{B} - \hat{A}\langle\hat{B}\rangle - \hat{B}\langle\hat{A}\rangle + \langle\hat{A}\rangle\langle\hat{B}\rangle)\Psi\rangle \\
&= \langle \Psi|\hat{A}\hat{B}\Psi\rangle - \langle\Psi|\hat{A}\langle\hat{B}\rangle\Psi\rangle - \langle\Psi|\hat{B}\langle\hat{A}\rangle\Psi\rangle + \langle\Psi|\langle\hat{A}\rangle\langle\hat{B}\rangle\Psi\rangle \\
&= \langle\hat{A}\hat{B}\rangle - \langle\hat{A}\rangle\langle\hat{B}\rangle - \langle\hat{A}\rangle\langle\hat{B}\rangle + \langle\hat{A}\rangle\langle\hat{B}\rangle \\
&= \langle\hat{A}\hat{B}\rangle - \langle\hat{A}\rangle\langle\hat{B}\rangle\,. \qquad (2.9)
\end{aligned}$$

Similarly it can be shown that

$$\langle g|f\rangle = \langle\hat{B}\hat{A}\rangle - \langle\hat{A}\rangle\langle\hat{B}\rangle. \qquad (2.10)$$

I insert these two results, Eqs. (2.9) and (2.10), into Eq. (2.8) to get

$$\langle f|g\rangle - \langle g|f\rangle = \langle\hat{A}\hat{B}\rangle - \langle\hat{A}\rangle\langle\hat{B}\rangle - \langle\hat{B}\hat{A}\rangle + \langle\hat{A}\rangle\langle\hat{B}\rangle = \langle[\hat{A},\hat{B}]\rangle \qquad (2.11)$$

and

$$\langle f|g\rangle + \langle g|f\rangle = \langle\hat{A}\hat{B}\rangle - \langle\hat{A}\rangle\langle\hat{B}\rangle + \langle\hat{B}\hat{A}\rangle - \langle\hat{A}\rangle\langle\hat{B}\rangle = \langle\{\hat{A},\hat{B}\}\rangle - 2\langle\hat{A}\rangle\langle\hat{B}\rangle. \qquad (2.12)$$

I now substitute Eqs. (2.11) and (2.12) back into Eq. (2.8) and get

$$|\langle f|g\rangle|^2 = \left(\frac{1}{2}\langle\{\hat{A},\hat{B}\}\rangle - \langle\hat{A}\rangle\langle\hat{B}\rangle\right)^2 + \left(\frac{1}{2i}\langle[\hat{A},\hat{B}]\rangle\right)^2. \qquad (2.13)$$

Substituting (2.13) into (2.6) I get the Schrödinger uncertainty relation

$$\boxed{\sigma_A\sigma_B \geq \sqrt{\left(\frac{1}{2}\langle\{\hat{A},\hat{B}\}\rangle - \langle\hat{A}\rangle\langle\hat{B}\rangle\right)^2 + \left(\frac{1}{2i}\langle[\hat{A},\hat{B}]\rangle\right)^2}}. \qquad (2.14)$$

2.3 Uncertainty for Mixed States

2.3.1 Mixed States, the Density Operator, and Uncertainty

So far I have considered only "pure" quantum states, e.g. $|f\rangle$ and $|g\rangle$. A pure state is one that can be described by a single ket vector, as in $|\psi\rangle = a_1|\psi_1\rangle + a_2|\psi_2\rangle$, where a_1 and a_2 are scalar quantities. In contrast, a mixed state is a statistical ensemble of pure states and cannot be represented by a single state vector, but must be represented by a density operator. Given a quantum system[1] in one of the states $|\psi_i\rangle$, with respective probabilities p_i, the general density operator ρ is defined [18] as

$$\rho \equiv \sum_i p_i |\psi_i\rangle\langle\psi_i|. \tag{2.15}$$

Compared to the pure state formalism of quantum mechanics, density operators are used to describe a much wider class of quantum states [22]. Not only can a density operator be used to represent a pure state (i.e. when every p_i but one is zero), it can be used when one deals with an ensemble of systems or when one is uncertain about the state of the system at hand. The density operator of a mixed state describes the statistical state of a quantum system, including both quantum and classical aspects—quantum uncertainty and classical randomness.

A translation of pure states into mixed states requires a few transformations. For the purposes of this thesis, I only discuss briefly how expectation values are expressed with density matrices. The expectation value of an arbitrary operator $\hat{A}$ changes such that

$$\langle \hat{A} \rangle \Longrightarrow Tr(\rho A) \tag{2.16}$$

where ρ is the density matrix that describes the mixed state and Tr denotes the trace.

[1] Here and throughout this thesis, I always choose an orthonormal basis.

The trace of an $n \times n$ matrix D with elements d_{ij} is defined as

$$Tr(D) = \sum_{i=1}^{n} d_{ii}\,,$$

which is the sum of the diagonal elements of the matrix D. The trace is invariant under a change of orthonormal basis.

How "mixed" a state is can be determined by its total polarization P. For spin 1/2, the polarization in a particular direction is defined as

$$P_i = \langle \sigma_i \rangle = Tr(\rho\sigma_i), \tag{2.17}$$

where $i = x, y, z$ and σ_i corresponds to the Pauli spin matrices. The total polarization P is given by

$$P = \sqrt{P_x^2 + P_y^2 + P_z^2}\,. \tag{2.18}$$

P has the range of $0 \le P \le 1$, where a polarization of $P = 0$ corresponds to a completely unpolarized or mixed state and $P = 1$ corresponds to a completely polarized or pure state. The general density operator for spin 1/2 in terms of polarization is given by

$$\rho = \frac{1}{2}\begin{pmatrix} 1 + P_z & P_x - iP_y \\ P_x + iP_y & 1 - P_z \end{pmatrix}. \tag{2.19}$$

For mixed states I can also parameterize this state inside the Bloch sphere with

$$P_x = P\sin\theta\cos\phi\,, \quad P_y = P\sin\theta\sin\phi\,, \quad \text{and} \quad P_z = P\cos\theta \tag{2.20}$$

where $0 \le \theta \le \pi$ and $0 \le \phi \le 2\pi$ are angles in spherical coordinates. I use this state in Eq. (2.19) along with the parameterizations of Eq. (2.20) in all my calculations of spin-1/2 mixed states.

Uncertainty relations also apply to the case of mixed states. In the language of mixed states, the uncertainty relation that is equivalent to the Robertson relation [23] is given by

$$\sigma_A\sigma_B \ge \frac{1}{2i}Tr(\rho[A, B])\,, \tag{2.21}$$

while the equivalent equation for the Schrödinger relation is

$$\sigma_A^2\sigma_B^2 \geq \left(\frac{1}{2}Tr(\rho\{A,B\}) - Tr(\rho A)Tr(\rho B)\right)^2 + \left(\frac{1}{2i}Tr(\rho[A,B])\right)^2, \tag{2.22}$$

as alluded to—but not presented—in Ballentine [23].

2.3.2 Schrödinger Uncertainty Relation For Mixed States

I now derive the Schrödinger uncertainty relation for mixed states. I initially follow Ballentine [23] to derive the Robertson uncertainty relation for mixed states, Eq. (2.21), but I extend it to derive the Schrödinger uncertainty relation for mixed states.

The standard deviations for Hermitian operators $\hat{A}$ and $\hat{B}$ are defined as $\sigma_A^2 = \langle\Psi|(\hat{A} - \langle\hat{A}\rangle)^2\Psi\rangle$ and $\sigma_B^2 = \langle\Psi|(\hat{B} - \langle\hat{B}\rangle)^2\Psi\rangle$. To simplify the calculations, I also define the operators $A_o = \hat{A} - \langle\hat{A}\rangle$ and $B_o = \hat{B} - \langle\hat{B}\rangle$. By these two definitions and that of the expectation value for mixed states, Eq. (2.16), I have

$$\sigma_A^2 = Tr(\rho A_o^2) \quad \text{and} \quad \sigma_B^2 = Tr(\rho B_o^2).$$

In a step reminiscent of that used for the derivation for pure states where I invoked the Schwarz inequality Eq. (2.5), I now use an inequality for mixed states. For any operator T the inequality [23]

$$Tr(\rho TT^\dagger) \geq 0 \tag{2.23}$$

holds, where $T^\dagger$ denotes the Hermitian conjugate of the operator T. I introduce two real parameters γ and ϵ in the following manner,

$$T = A_o + (\gamma + i\epsilon)B_o \quad \text{and} \quad T^\dagger = A_o + (\gamma - i\epsilon)B_o \tag{2.24}$$

where A_o and B_o are Hermitian. In order to use Eq. (2.23), I need the product of T

and $T^\dagger$

$$\begin{aligned} TT^\dagger &= (A_o + \gamma B_o + i\epsilon B_o)(A_o + \gamma B_o - i\epsilon B_o) \\ &= A_o^2 + \gamma A_o B_o - i\epsilon A_o B_o + \gamma B_o A_o + \gamma^2 B_o^2 - i\epsilon\gamma B_o^2 + i\epsilon B_o A_o + i\epsilon\gamma B_o^2 + \epsilon^2 B_o^2 \\ &= A_o^2 + (\gamma^2 + \epsilon^2)B_o^2 + \gamma\{A_o, B_o\} - i\epsilon[A_o, B_o]. \end{aligned}$$

Now plugging this into Eq. (2.23) I have

$$\begin{aligned} 0 &\leq Tr(\rho TT^\dagger) \\ 0 &\leq Tr(\rho A_o^2) + (\gamma^2 + \epsilon^2)Tr(\rho B_o^2) + \gamma Tr(\rho\{A_o, B_o\}) - i\epsilon Tr(\rho[A_o, B_o]). \end{aligned} \tag{2.25}$$

I seek to minimize this expression for γ and ϵ in order to optimize the uncertainty relation. Thus

$$\frac{\partial Tr(\rho TT^\dagger)}{\partial\gamma} = 0 \quad \text{and} \quad \frac{\partial Tr(\rho TT^\dagger)}{\partial\epsilon} = 0$$

implies

$$2\gamma Tr(\rho B_o^2) + Tr(\rho\{A_o, B_o\}) = 0 \quad \text{and} \quad 2\epsilon Tr(\rho B_o^2) - iTr(\rho[A_o, B_o]) = 0\,.$$

I now solve for γ and ϵ and find that

$$\begin{aligned} 2\gamma Tr(\rho B_o^2) &= -Tr(\rho\{A_o, B_o\}) \\ \gamma &= -\frac{Tr(\rho\{A_o, B_o\})}{2Tr(\rho B_o^2)} \end{aligned}$$

and also,

$$\begin{aligned} 2\epsilon Tr(\rho B_o^2) &= iTr(\rho[A_o, B_o]) \\ \epsilon &= \frac{iTr(\rho[A_o, B_o])}{2Tr(\rho B_o^2)}. \end{aligned}$$

Now I substitute the minimal values of γ and ϵ that I obtained back into Eq. (2.25) and simplify the inequality to get

$$Tr(\rho A_o^2)Tr(\rho B_o^2) \geq \frac{1}{4}\left(\Big(Tr(\rho\{A_o, B_o\})\Big)^2 - \Big(Tr(\rho[A_o, B_o])\Big)^2\right). \tag{2.26}$$

At the beginning of the proof I made the substitutions $A_o = A - \langle A \rangle$ or equally $A_o = A - Tr(\rho A)$ and $B_o = B - \langle B \rangle$ or $B_o = B - Tr(\rho B)$, so now I put these substitutions back into Eq. (2.26). I first work out the left-hand-side of (2.26), $Tr(\rho A_o^2)Tr(\rho B_o^2)$, which becomes

$$\begin{aligned}
&Tr\Big(\rho\big(A^2 - 2Tr(\rho A)A + \big(Tr(\rho A)\big)^2\big)Tr\Big(\rho\big(B^2 - 2Tr(\rho B)B + \big(Tr(\rho B)\big)^2\Big) \\
=&\Big(Tr(\rho A^2) - 2Tr(\rho A)Tr(\rho A) + \big(Tr(\rho A)\big)^2\Big)\Big(Tr(\rho B^2) - 2Tr(\rho B)Tr(\rho B) + \big(Tr(\rho B)\big)^2\Big) \\
=&\Big(Tr(\rho A^2) - \big(Tr(\rho A)\big)^2\Big)\Big(Tr(\rho B^2) - \big(Tr(\rho B)\big)^2\Big) \\
=&\sigma_A^2\sigma_B^2 \,. \qquad (2.27)
\end{aligned}$$

I next work out the anticommutator term in the right hand side of Eq. (2.26),

$$\begin{aligned}
\{A_o, B_o\} =&\Big(A - Tr(\rho A)\Big)\Big(B - Tr(\rho B)\Big) + \Big(B - Tr(\rho B)\Big)\Big(A - Tr(\rho A)\Big) \\
=&AB - Tr(\rho A)B - Tr(\rho B)A + Tr(\rho A)Tr(\rho B) \\
&+ BA - Tr(\rho B)A - Tr(\rho A)B + Tr(\rho A)Tr(\rho B).
\end{aligned}$$

And now I take the expectation value for mixed states of the anticommutator, as in Eq. (2.16),

$$\begin{aligned}
Tr\big(\rho\{A_o, B_o\}\big) =&Tr(\rho AB) - Tr(\rho A)Tr(\rho B) - Tr(\rho B)Tr(\rho A) + Tr(\rho A)Tr(\rho B) \\
&+ Tr(\rho BA) - Tr(\rho B)Tr(\rho A) - Tr(\rho A)Tr(\rho B) + Tr(\rho A)Tr(\rho B) \\
=&Tr(\rho AB) + Tr(\rho BA) - 2Tr(\rho A)Tr(\rho B) \\
=&Tr\big(\rho\{A, B\}\big) - 2Tr(\rho A)Tr(\rho B). \qquad (2.28)
\end{aligned}$$

The commutator yields

$$\begin{aligned}
[A_o, B_o] =&\Big(A - Tr(\rho A)\Big)\Big(B - Tr(\rho B)\Big) - \Big(B - Tr(\rho B)\Big)\Big(A - Tr(\rho A)\Big) \\
=&AB - Tr(\rho A)B - Tr(\rho B)A + Tr(\rho A)Tr(\rho B) \\
&- BA + Tr(\rho B)A + Tr(\rho A)B - Tr(\rho A)Tr(\rho B)
\end{aligned}$$

and taking the expectation value I have,

$$\begin{aligned} Tr\big(\rho[A_o, B_o]\big) =& Tr(\rho AB) - Tr(\rho A)Tr(\rho B) - Tr(\rho B)Tr(\rho A) + Tr(\rho A)Tr(\rho B) \\ & - Tr(\rho BA) + Tr(\rho B)Tr(\rho A) + Tr(\rho A)Tr(\rho B) - Tr(\rho A)Tr(\rho B) \\ =& Tr(\rho AB) - Tr(\rho BA) \\ =& Tr\big(\rho[A, B]\big). \end{aligned} \tag{2.29}$$

Finally, I combine Eqs. (2.26)–(2.29) to get

$$\sigma_A^2\sigma_B^2 \geq \frac{1}{4}\Big(Tr(\rho\{A, B\}) - 2Tr(\rho A)Tr(\rho B)\Big)^2 - \frac{1}{4}\Big(Tr(\rho[A, B])\Big)^2,$$

which can be written as

$$\boxed{\sigma_A^2\sigma_B^2 \geq \left(\frac{1}{2}Tr(\rho\{A, B\}) - Tr(\rho A)Tr(\rho B)\right)^2 + \left(\frac{1}{2i}Tr(\rho[A, B])\right)^2}, \tag{2.30}$$

which is the Schrödinger uncertainty relation for mixed states.

2.4 Discussion of Uncertainty and Uncertainty Relations

An analysis of the derivations contained in this chapter reveals that uncertainty first comes into play with the Schwarz inequality (2.5) and the related inequality for mixed states (2.23). The Schwarz inequality was used first by Weyl in his 1928 derivation of

$$\sigma_x\sigma_p \geq \frac{\hbar}{2}$$

in which he sought (at the suggestion of Wolfgang Pauli) to relate the two standard deviations σ_x and σ_p [12]. The Schwarz inequality was also used by Robertson in his 1929 derivation and Schrödinger in his 1930 derivation, who both cite Weyl [2, 3].

Schrödinger's method of derivation differed from that of Robertson. The critical step that differentiates the two is Schrödinger's use of the fact that the product of

two Hermitian operators is not in general Hermitian, but can be split [24] into a "symmetric product and half its commutator":

$$AB = \frac{AB + BA}{2} + \frac{AB - BA}{2}\,. \tag{2.31}$$

Schrödinger then comments that this splitting corresponds to a splitting of a complex number into real and imaginary parts, and thus an expectation value can also be split into real and imaginary parts. This corresponds directly to the step involved in Eq. (2.7) of the pure state derivation and Eq. (2.24) of the mixed state derivation. If one takes only the imaginary part, one recovers the Robertson relation; if one takes both the real and imaginary parts, the Schrödinger relation results.[2]

The additional term in the Schrödinger relation, known as the "covariance," was also discussed by Schrödinger (cf. Eqs. (2.2), (2.14), and (2.30)). In an English translation [24] of the original German paper [3], Schrödinger calls the covariance the "mean deviations product." Schrödinger says that in classical probability theory, a vanishing mean deviations product is a necessary but not sufficient condition for two values to fluctuate independently. He then asserts that because "canonically conjugate quantum variables have some 'independence,'" one might suppose that the mean deviations product has a "vanishing expectation value." However, he notes, "this is not the case." Schrödinger then goes on to discuss situations in which the covariance or "mean deviations product" is non-vanishing.

As pointed out originally by Schrödinger, the Schrödinger uncertainty relation often has the effect of raising the lower bound on uncertainty. Because the added terms, viz., the anticommutator $\{A, B\}$ and the product of expectation values $\langle A\rangle\langle B\rangle$, are squared, the Schrödinger additions are either positive or zero. This will obviously

[2]Though Schrödinger's original method of derivation for his uncertainty relation differs from that shown in Section 2.2, the key elements of the derivation are the same.

either increase the uncertainty by some amount, or make no difference. Both of these scenarios will be discussed and examples will be shown in Chapter 3 of this thesis.

Chapter 3

Uncertainty Data

3.1 Uncertainty in One Dimension

Despite the fact that the Schrödinger uncertainty relation is of a different form than the Robertson uncertainty relation, some authors of both textbooks and papers dismiss the Schrödinger uncertainty relation[1] because in their estimation it "doesn't help much" (see [9], pg. 128). A perfunctory glance would seem to justify this position; comparing the calculations of uncertainty using the Schrödinger and Robertson relations for $\hat{x}$ and $\hat{p}$ in simple cases gives the uncertainty limit of $\hbar/2$, as in Eq. (2.1) (see Tables 3.1, 3.2, and 3.3). Yet for many quantum operators of more complexity, in these same simple systems (e.g., $\hat{x}+\hat{p}$ and $\frac{1}{2}(\hat{x}\hat{p}+\hat{p}\hat{x})$) or for operators for spin systems (e.g., $\hat{S}_x$, $\hat{S}_y$, and $\hat{S}_x+\hat{S}_y$), the difference between Robertson and Schrödinger is significant. These differences will be demonstrated in this chapter.

[1] Angelow discusses this neglect at length in [20], and then discusses certain experimental scenarios where the Schrödinger uncertainty relation is necessary.

3.1.1 The Infinite Square Well

A particle confined in an infinite square well potential of width L

$$V(x) = \begin{cases} 0 & \text{if } 0 \le x \le L \\ \infty & \text{otherwise} \end{cases}$$

has stationary states given by

$$\psi_n(x) = \sqrt{\frac{2}{L}} \sin\Big(\frac{2\pi n x}{L}\Big). \tag{3.1}$$

Using the wave function defined in Eq. (3.1) I calculate the product of standard deviations and the Robertson and Schrödinger uncertainties for the position and momentum operator pairs $(\hat{x}, \hat{p})$, $(\frac{1}{2}(\hat{x}\hat{p} + \hat{p}\hat{x}), \hat{p})$, and $(\hat{x} + \hat{p}, \hat{p})$; I choose these pairs for all the calculations in this and the following sections in one dimension because they give a spectrum of results. Table 3.1 summarizes the results of the calculations and a discussion of these results is contained Section 3.2. In viewing the results, it is important to note that because the operators are atypical compared to those found in traditional textbook calculations, the units of the results differ from common calculations as well.

Table 3.1 Summary of results for the Infinite Square Well. The entries in the columns under $\hat{A}$ and $\hat{B}$ are operators. The entries under $\sigma_A\sigma_B$ are the standard deviations for the particular operators. Here n corresponds to positive integer values used in the function for an infinite square well, Eq. (3.1).

$\hat{A}$	$\hat{B}$	$\sigma_A\sigma_B$	$\frac{1}{2i}\langle[\hat{A},\hat{B}]\rangle$	$\sqrt{\Big(\frac{1}{2}\langle\{\hat{A},\hat{B}\}\rangle - \langle\hat{A}\rangle\langle\hat{B}\rangle\Big)^2 + \Big(\frac{1}{2i}\langle[\hat{A},\hat{B}]\rangle\Big)^2}$
x	p	$\frac{\hbar}{2}\sqrt{-2 + \frac{n^2\pi^2}{3}}$	$\frac{\hbar}{2}$	$\frac{\hbar}{2}$
$\frac{1}{2}(xp + px)$	p	$\frac{n\pi\hbar^2}{2L}\sqrt{1 - \frac{L}{2} + n^2\pi^2}$	0	$\frac{n^2\pi^2\hbar^2}{2L}$
$x + p$	p	$\frac{\hbar}{2}\sqrt{-2 + \frac{n^2\pi^2}{3} + \frac{4n^4\pi^4\hbar^2}{L^4}}$	$\frac{\hbar}{2}$	$\sqrt{\frac{\hbar^2}{4} + \frac{n^4\pi^4\hbar^4}{L^4}}$

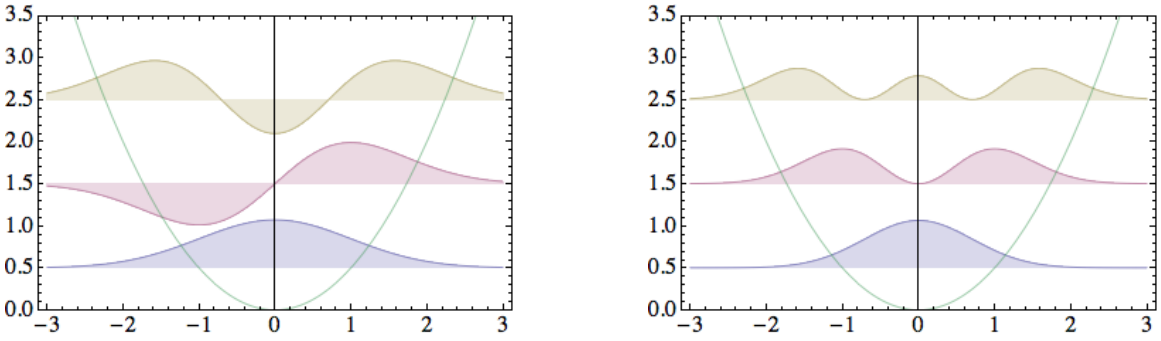

Figure 3.1 The figure on the left is a plot of $\psi_n(x)$ given in Eq. (3.3), while the figure on the right is a plot of $|\psi_n(x)|^2$. Both of these plots are for values $n = 0, 1, 2$.

3.1.2 The Harmonic Oscillator

For the harmonic oscillator, a particle is under the influence of the potential

$$V(x) = \frac{1}{2}m\omega^2 x^2 \,, \tag{3.2}$$

where ω is the angular frequency and m is the mass of the particle. The stationary solutions to the Schrödinger equation for this potential are the wave functions

$$\psi_n(x) = \left(\frac{m\omega}{\pi\hbar}\right)^{1/4} \frac{1}{\sqrt{2^n n!}} H_n(\xi) e^{\xi^2/2} \,, \tag{3.3}$$

where $\xi \equiv \sqrt{\frac{m\omega}{\hbar}}x$ and $H_n(\xi)$ are Hermite polynomials. As n increases, the calculations of uncertainties increase rapidly in complexity; therefore we choose to summarize only results for $n = 0, 1, 2$ in Table 3.2. As a reference, plots of $\psi_n(x)$ and $|\psi_n(x)|^2$ for $n = 0, 1, 2$ are shown in Fig. 3.1. A discussion of the results is contained in the discussion section for one dimension uncertainty, Section 3.2.

3.1.3 The Free-Particle Wave Packet

For the free-particle wave packet, $V(x) = 0$, I consider both a Gaussian and a non-Gaussian wave packet. A particular normalized Gaussian wave packet centered

Table 3.2 Summary of results for the the Harmonic Oscillator for $n = 0, 1, 2$.

n	$\hat{A}$	$\hat{B}$	$\sigma_A\sigma_B$	$\frac{1}{2i}\langle[\hat{A},\hat{B}]\rangle$	$\sqrt{\left(\frac{1}{2}\langle\{\hat{A},\hat{B}\}\rangle - \langle\hat{A}\rangle\langle\hat{B}\rangle\right)^2 + \left(\frac{1}{2i}\langle[\hat{A},\hat{B}]\rangle\right)^2}$
0	x	p	$\frac{\hbar}{2}$	$\frac{\hbar}{2}$	$\frac{\hbar}{2}$
1	x	p	$\frac{3\hbar}{2}$	$\frac{\hbar}{2}$	$\frac{\hbar}{2}$
2	x	p	$\frac{5\hbar}{2}$	$\frac{\hbar}{2}$	$\frac{\hbar}{2}$
0	$\frac{1}{2}(xp+px)$	p	$\frac{1}{4}\sqrt{\frac{7}{2}m\omega\hbar^3}$	0	0
1	$\frac{1}{2}(xp+px)$	p	$\frac{1}{4}\sqrt{\frac{57}{2}m\omega\hbar^3}$	0	0
2	$\frac{1}{2}(xp+px)$	p	$\frac{1}{4}\sqrt{\frac{215}{2}m\omega\hbar^3}$	0	0
0	$x+p$	p	$\frac{1}{2}\hbar\sqrt{1+m^2\omega^2}$	$\frac{\hbar}{2}$	$\frac{1}{2}\hbar\sqrt{1+m^2\omega^2}$
1	$x+p$	p	$\frac{3}{2}\hbar\sqrt{1+m^2\omega^2}$	$\frac{\hbar}{2}$	$\frac{1}{2}\hbar\sqrt{1+9m^2\omega^2}$
2	$x+p$	p	$\frac{5}{2}\hbar\sqrt{1+m^2\omega^2}$	$\frac{\hbar}{2}$	$\frac{1}{2}\hbar\sqrt{1+25m^2\omega^2}$

around $x = 0$ is given by

$$\psi = \left(\frac{2}{\pi}\right)^{1/4} e^{-x^2}, \tag{3.4}$$

while an example of a normalized, yet non-Gaussian wave packet is given by

$$\psi = \frac{4}{\sqrt{3}}\left(\frac{2}{\pi}\right)^{1/4} x^2 e^{-x^2}. \tag{3.5}$$

There is nothing special about this wave packet except that it is non-Gaussian and adequately demonstrates the difference between a Gaussian and non-Gaussian wave packet. Graphs of Eqs. (3.4) and (3.5) are shown in Fig. 3.2. For both Eq. (3.4) and Eq. (3.5) I calculate values of uncertainty for the Robertson and Schrödinger relations and summarize these results in Table 3.3. A discussion of the results is contained in the discussion section for one dimension uncertainty, Section 3.2.

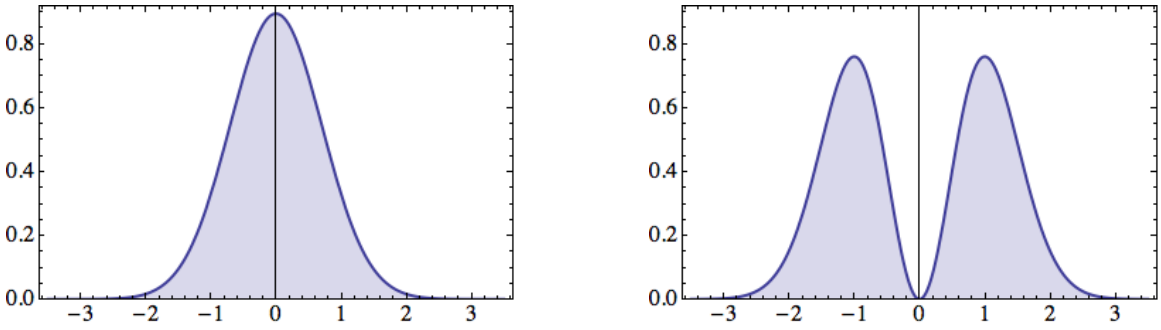

Figure 3.2 The plot on the left is of the Gaussian wave packet defined by Eq. (3.4) and the plot on the right is of the non-Gaussian wave packet defined by Eq. (3.5).

Table 3.3 Summary of results for the Gaussian free-particle wave packet defined by Eq. (3.4).

$\hat{A}$	$\hat{B}$	$\sigma_A\sigma_B$	$\frac{1}{2i}\langle[\hat{A},\hat{B}]\rangle$	$\sqrt{\left(\frac{1}{2}\langle\{\hat{A},\hat{B}\}\rangle - \langle\hat{A}\rangle\langle\hat{B}\rangle\right)^2 + \left(\frac{1}{2i}\langle[\hat{A},\hat{B}]\rangle\right)^2}$
x	p	$\frac{\hbar}{2}$	$\frac{\hbar}{2}$	$\frac{\hbar}{2}$
$\frac{1}{2}(xp+px)$	p	$\frac{\sqrt{7}}{4}\hbar^2$	0	0
$x+p$	p	$\hbar\sqrt{\frac{1}{4}+\hbar^2}$	$\frac{\hbar}{2}$	$\hbar\sqrt{\frac{1}{4}+\hbar^2}$

Table 3.4 Summary of results for the non-Gaussian free-particle wave packet defined by Eq. (3.5).

$\hat{A}$	$\hat{B}$	$\sigma_A\sigma_B$	$\frac{1}{2i}\langle[\hat{A},\hat{B}]\rangle$	$\sqrt{\left(\frac{1}{2}\langle\{\hat{A},\hat{B}\}\rangle - \langle\hat{A}\rangle\langle\hat{B}\rangle\right)^2 + \left(\frac{1}{2i}\langle[\hat{A},\hat{B}]\rangle\right)^2}$
x	p	$\frac{1}{2}\sqrt{\frac{35}{3}}\hbar$	$\frac{\hbar}{2}$	$\frac{\hbar}{2}$
$\frac{1}{2}(xp+px)$	p	$\frac{1}{4}\sqrt{\frac{217}{3}}\hbar^2$	0	0
$x+p$	p	$\frac{\sqrt{7}}{6}\hbar\sqrt{15+28\hbar^2}$	$\frac{\hbar}{2}$	$\frac{1}{6}\hbar\sqrt{9+196\hbar^2}$

3.2 Discussion of One-Dimensional Data

For certain quantum systems in one dimension, the Robertson relation is clearly insufficient. It is an incomplete relation and often gives incomplete results, as evident from the results shown in Tables (3.1), (3.2), (3.3), and (3.4). Yet in presenting the disparities, I have sought to give a spectrum of scenarios. Consider, for example, the values in Table (3.2): for $\hat{x}$ and $\hat{p}$ both Robertson and Schrödinger are the same, for $\frac{1}{2}(\hat{x}\hat{p} + \hat{p}\hat{x})$ and $\hat{p}$ both are zero, and for $\hat{x} + \hat{p}$ and $\hat{p}$ the Schrödinger relation effectively raises the lower bound on uncertainty. With greater operator complexity comes greater difference between Robertson and Schrödinger. As briefly discussed in Section 2.4, this greater complexity increases the covariance and thus widens the difference between the two uncertainty relations.

3.3 Uncertainty for Angular Momentum

The differences between the Robertson and Schrödinger uncertainty relations also extend to situations in three dimensions. In the following sections I will discuss the concept of a general state (see Fig. 3.3) and the process of calculating angular momentum uncertainty for $j = 1/2$. I will show plots of these uncertainties for some examples with $j = 1/2$ and $j = 2$. This will be followed by a summary of all the results that I found for $j = 1/2, 1, 3/2, 2$. Lastly, I will discuss how uncertainty is affected for the $j = 1/2$ case when the parameterized mixed state, Eq. (2.19), is used in the calculations of uncertainty.

In these sections I do not included calculations and results for the three-dimensional extensions of those systems covered in the previous sections, such as for the three-dimensional square well or harmonic oscillator (where instead of just considering a single dimension, one could also consider position in (x, y, z) or momentum in

(p_x, p_y, p_z)). The reason why I have not included these calculations is that there were no significantly new or surprising results from working in three dimensions: the results were essentially the same as when I considered position and momentum in one dimension. For example, in the three-dimensional square well the results for operator pairs $(\hat{x}, \hat{p_x})$ give exactly the same results as in the one-dimensional case (see Table 3.1). If the operator pairs are changed to $(\hat{x}, \hat{p_y})$ and $(\hat{y} + \hat{p_x}, \hat{p_y})$, the results change to:

$$\Delta\hat{x}\Delta\hat{p_y} = \frac{m\hbar}{2l}\sqrt{-2 + \frac{l^2\pi^2}{3}} \ , \ \Delta(\hat{y} + \hat{p_x})\Delta\hat{p_y} = \frac{\hbar}{2\sqrt{3}}\sqrt{-6 + m^2\Big(\pi^2 + \frac{12l^2\pi^4\hbar^2}{a^4}\Big)}$$

$$\text{Robertson}_{(\hat{x},\hat{p_y})} = 0 \ , \ \text{Robertson}_{(\hat{y}+\hat{p_x},\hat{p_y})} = \frac{\hbar}{2}$$

$$\text{Schrödinger}_{(\hat{x},\hat{p_y})} = 0 \ , \ \text{Schrödinger}_{(\hat{y}+\hat{p_x},\hat{p_y})} = \frac{\hbar}{2} \, ,$$

which are somewhat more complex, but not strikingly new. As will be shown, the results for angular momentum are visually and mathematically more interesting.

3.3.1 Spin-1/2 Uncertainty

To calculate angular momentum uncertainty in a way more general than simply choosing single eigenstates, I use generalized states (see Fig. 3.3); these states are functions of the spherical angles (θ, ϕ), and along with a magnitude, they determine any state in the space. I use these general states in my calculations of uncertainty by associating an uncertainty with the general eigenstate after calculating all the expectation values implied by the Robertson and Schrödinger uncertainty relations. Combining all these magnitudes of uncertainty gives us the spherical plots given in the figures of the following sections.[2]

[2] Just like in the calculations in one dimension, all the results are in terms of $\hbar$. For computational purposes, all the figures in the angular momentum sections are computed with $\hbar = 1$.

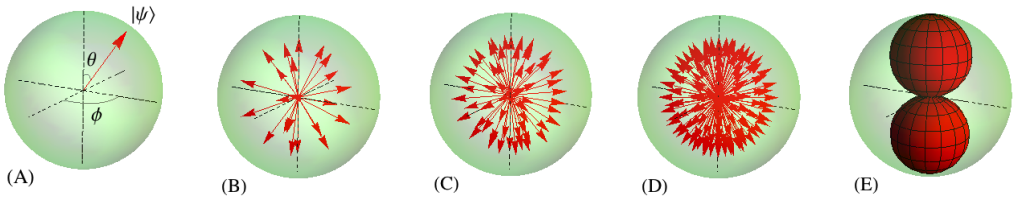

Figure 3.3 Representation and use of a general quantum state. (A) Like a vector, any state $|\psi\rangle$ can be denoted by a direction using the spherical angles (θ, ϕ) and a magnitude. A general state represents any possible state in the space. (B)-(D) Computing with a general state is equivalent to performing a particular computation for all possible specific states and combining all those results together. (E) The result of computing uncertainty using a general state. For any specific state, designated by some (θ, ϕ), the magnitude or value at the surface of the spherical object shown in (E) is the value of uncertainty for that specific state.

I proceed to construct the $\mathbf{J}_r^{(1/2)}$ matrix which represents the spin angular momentum for an arbitrary direction $\hat{r}$. I begin with the unit vector

$$\hat{r} = (\sin\theta\cos\phi, \sin\theta\sin\phi, \cos\theta)$$

and the total spin angular momentum vector

$$\mathbf{S} = (S_x, S_y, S_z)\,,$$

where $S_i = \sigma_i \hbar/2$ are the spin operators. Taking the dot product and simplifying,

$$\begin{aligned}\mathbf{J}_r^{(1/2)} = \mathbf{S}\cdot\hat{r} =& S_x\sin\theta\cos\phi + S_y\sin\theta\sin\phi + S_z\cos\theta \\ =& \frac{\hbar}{2}\begin{pmatrix} \cos\theta & \sin\theta(\cos\phi - i\sin\phi) \\ \sin\theta(\cos\phi + i\sin\phi) & -\cos\theta \end{pmatrix} \\ =& \frac{\hbar}{2}\begin{pmatrix} \cos\theta & e^{-i\phi}\sin\theta \\ e^{i\phi}\sin\theta & -\cos\theta \end{pmatrix}, \end{aligned} \tag{3.6}$$

which is the desired matrix. The eigenvalues of this matrix are $\pm\hbar/2$ with the corresponding eigenvectors

$$\chi_+^{(r)} = \begin{pmatrix} \cos(\theta/2) \\ e^{i\phi}\sin(\theta/2) \end{pmatrix} \qquad \text{and} \qquad \chi_-^{(r)} = \begin{pmatrix} e^{-i\phi}\sin(\theta/2) \\ -\cos(\theta/2) \end{pmatrix}. \tag{3.7}$$

I can use either of these eigenvectors as the states with which I take expectation values for calculating the Robertson and Schrödinger uncertainties for spin 1/2.

I now outline the calculations of the Robertson and Schrödinger uncertainties for spin. The left hand side of Eqs. (2.2) and (2.14) is the same, the product of standard deviations is given by

$$\sigma_{S_x}\sigma_{S_y} = \sqrt{\Big(\langle \hat{S}_x{}^2\rangle - \langle \hat{S}_x\rangle^2\Big)\Big(\langle \hat{S}_y{}^2\rangle - \langle \hat{S}_y\rangle^2\Big)}\,. \tag{3.8}$$

In calculating the product of standard deviations, I performed the expectation values implied by Eq. (3.8) using the general spin state $\chi_+^{(r)}$ given in Eq. (3.7) (for spin 1/2, the results are the same if I used $\chi_-^{(r)}$ instead). I followed the same procedure for the Robertson uncertainty

$$\frac{1}{2i}\langle[\hat{S}_x, \hat{S}_y]\rangle \tag{3.9}$$

and the Schrödinger uncertainty

$$\sqrt{\Big(\frac{1}{2}\langle\{\hat{S}_x, \hat{S}_y\}\rangle - \langle\hat{S}_x\rangle\langle\hat{S}_y\rangle\Big)^2 + \Big(\frac{1}{2i}\langle[\hat{S}_x, \hat{S}_y]\rangle\Big)^2}. \tag{3.10}$$

After performing the calculations outlined in the previous paragraphs, I obtain functions representing uncertainty for different incompatible operators of spin 1/2. These uncertainties are functions of θ and ϕ and thus can be represented by plots in spherical coordinates. Figure 3.4 is a plot of uncertainty for the two incompatible spin operators $\hat{S}_x$ and $\hat{S}_y$, and Figure 3.5 is a plot for the two incompatible spin operators $\hat{S}_x$ and $\hat{S}_x + \hat{S}_y$. In each of the figures, the magnitude associated with a particular direction (θ, ϕ) is the uncertainty for a state in that particular direction.

3.3.2 Angular Momentum Uncertainty

I also calculate angular momentum uncertainties for $j = 1, 3/2, 2$. The process is essentially the same for calculating uncertainties of higher j: I construct the matrices

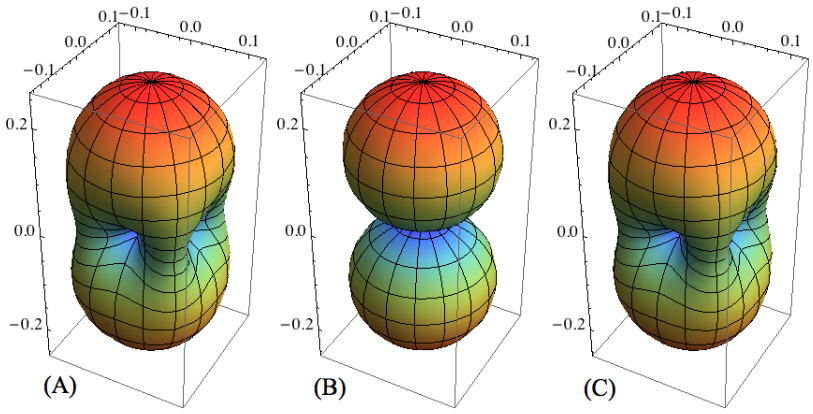

Figure 3.4 The magnitude of uncertainty for standard deviations (A), Robertson (B), and Schrödinger (C) uncertainty relations for spin $\frac{1}{2}$. $(A) = \sigma_{S_x}\sigma_{S_y}$, $(B) = \frac{1}{2i}\langle[\hat{S}_x, \hat{S}_y]\rangle$, $(C) = \sqrt{\left(\frac{1}{2}\langle\{\hat{S}_x, \hat{S}_y\}\rangle - \langle\hat{S}_x\rangle\langle\hat{S}_y\rangle\right)^2 + \left(\frac{1}{2i}\langle[\hat{S}_x, \hat{S}_y]\rangle\right)^2}$. These are plotted in spherical coordinates (θ, ϕ) with the amount of uncertainty in any particular direction corresponding to the value shown by the graph in that direction. The Robertson relation (B) is missing important segments that Schrödinger in (C) picks up. The Schrödinger relation accounts for all the uncertainty predicted by the product of the standard deviations.

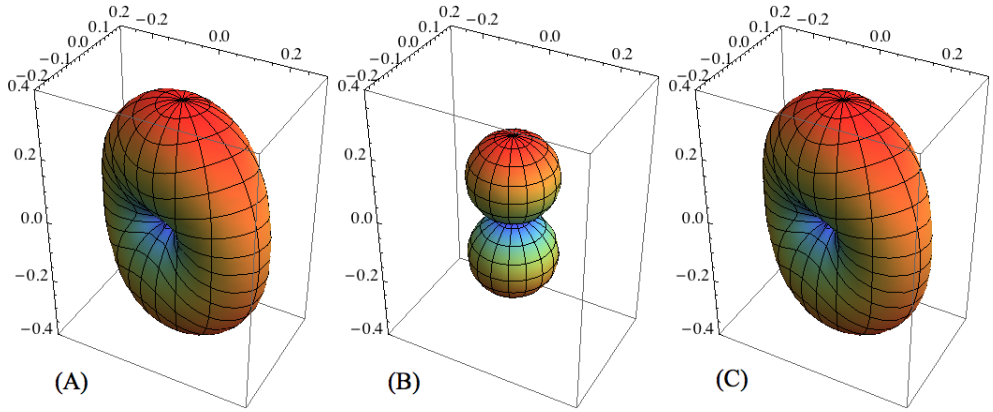

Figure 3.5 The magnitude of uncertainty for sums of operators for the case of spin $\frac{1}{2}$. $(A) = \sigma_{S_x+S_y}\sigma_{S_y}$, $(B) = \frac{1}{2i}\left(\langle[\hat{S}_x + \hat{S}_y, \hat{S}_y]\rangle\right)$, $(C) = \sqrt{\left(\frac{1}{2}\langle\{\hat{S}_x + \hat{S}_y, \hat{S}_y\}\rangle - \langle\hat{S}_x + \hat{S}_y\rangle\langle\hat{S}_y\rangle\right)^2 + \left(\frac{1}{2i}\langle[\hat{S}_x + \hat{S}_y, \hat{S}_y]\rangle\right)^2}$. The Robertson uncertainty relation (B) is missing essential information. The Schrödinger uncertainty relation (C) accounts for all the uncertainty predicted by the product of the standard deviations.

$\mathbf{J}_r^{(1)}$, $\mathbf{J}_r^{(3/2)}$, and $\mathbf{J}_r^{(2)}$, which represent the angular momentum in an arbitrary direction $\hat{r}$ (these matrices are given explicitly in Appendix A); I find their eigenvalues and eigenvectors; and I use the eigenvectors as general states in calculating the Robertson and Schrödinger uncertainties. Because of the complexity of the eigenvectors, I found it most convenient to perform all the calculations and the plotting numerically (see Appendix B for the *Mathematica* code). The results of these calculations are summarized in Table 3.5.

3.3.3 Spin Mixed State Uncertainty

The figures and discussion up to this point in Chapter 3 have only been for "pure" quantum states, e.g. $|f\rangle$ and $|g\rangle$. As discussed in Chapter 2, a mixed state is different from a pure state in that it is a statistical ensemble of pure states and cannot be represented by a single state vector, but must be represented by a density operator. Compared to the pure state formalism of quantum mechanics, density operators are used to describe a much wider class of quantum states [22]. These reasons make density operators particularly useful for practical applications of quantum mechanics.

As discussed in Chapter 2, uncertainty relations apply to mixed states as well. To illustrate the effects of mixed state uncertainty relations (Eqs. (2.21) and (2.30)), I show the results of computing some of the same spin-1/2 operator uncertainties that I did in Section 3.3.1. These uncertainties are shown in Figs. 3.6, 3.7, and 3.8. Like the spin-1/2 examples show in Section 3.3.1, the Schrödinger relation accounts for more uncertainty, raising the lower bound from the level of the Robertson relation. An additional insight observable from the results on mixed states is that the purer the state, the higher the uncertainty.

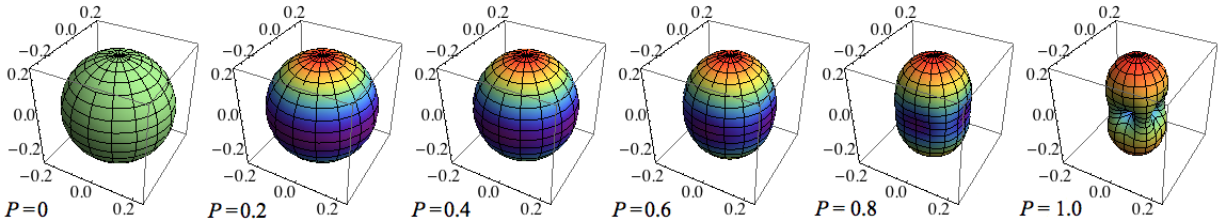

Figure 3.6 Uncertainty for the product of the standard deviations, $\sigma_{S_x}\sigma_{S_y}$. These are plotted in spherical coordinates (θ, ϕ) with the amount of uncertainty in any particular direction corresponding to the value shown by the graph in that direction. The six graphs correspond to six different values of total polarization, P, the measure of how "mixed" a state is. A polarization of $P = 0$ corresponds to a completely unpolarized or mixed state, and $P = 1$ corresponds to a completely polarized or pure state.

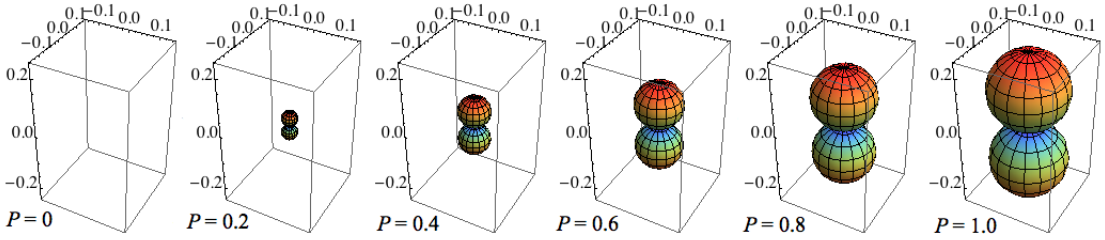

Figure 3.7 Uncertainty for the Robertson relation $\frac{1}{2i}\langle[\hat{S}_x, \hat{S}_y]\rangle$. These are plotted in spherical coordinates (θ, ϕ), and the six graphs correspond to six different values of polarization, P.

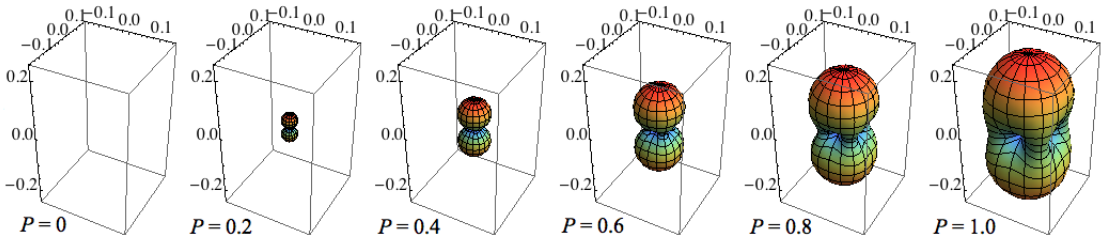

Figure 3.8 Uncertainty for the Schrödinger relation $\sqrt{\left(\frac{1}{2}\langle\{\hat{S}_x, \hat{S}_y\}\rangle - \langle\hat{S}_x\rangle\langle\hat{S}_y\rangle\right)^2 + \left(\frac{1}{2i}\langle[\hat{S}_x, \hat{S}_y]\rangle\right)^2}$. These are plotted in spherical coordinates (θ, ϕ) and the six graphs correspond to six different values of polarization, P.

Table 3.5 A summary of all results for angular momentum uncertainties. The figures in this table represent the general shape of the individual graphs of uncertainty, while the maximum values of uncertainty are indicated under $|Width|$ and $|Height|$ which values are measured from the origin of the corresponding figure. The variable j is the total angular momentum, corresponding to the superscript number of the matrices $\mathbf{J}_r^{(1/2)}$, $\mathbf{J}_r^{(1)}$, $\mathbf{J}_r^{(3/2)}$, and $\mathbf{J}_r^{(2)}$. The states used in the calculations were eigenvectors of these matrices with corresponding eigenvalue m indicated in the table.

j	m	$\sigma_{J_x^{(l)}}\sigma_{J_y^{(l)}}$	$\|Width\|$	$\|Height\|$	Robertson	$\|Width\|$	$\|Height\|$	Schrödinger	$\|Width\|$	$\|Height\|$
2	± 2	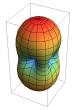	0.5	1.0	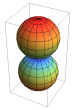	0.5	1.0	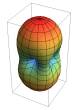	0.5	1.0
2	± 1	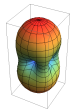	1.2	2.5	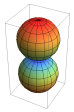	0.25	0.5		0.85	0.5
2	0	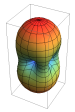	1.4	3.0	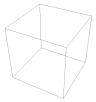	0.0	0.0		1.0	0.5
$\frac{3}{2}$	$\pm\frac{3}{2}$	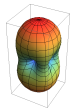	0.35	0.75	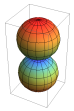	0.35	0.75	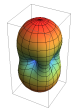	0.35	0.75
$\frac{3}{2}$	$\pm\frac{1}{2}$	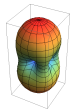	0.8	1.65	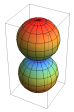	0.12	0.25		0.6	0.3
1	± 1	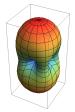	0.25	0.5	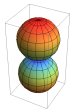	0.25	0.5	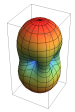	0.25	0.5
1	0	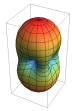	0.5	1.0	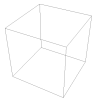	0.0	0.0		0.35	0.18
$\frac{1}{2}$	$\pm\frac{1}{2}$	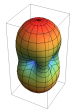	0.12	0.25	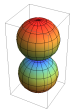	0.12	0.25	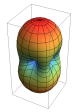	0.12	0.25

3.4 Discussion of Angular Momentum Data

The overall effect of the Schrödinger relation is often to raise the lower bound of uncertainty. This is the case for both pure and mixed states. The differences between the two uncertainty relations also become more pronounced with larger values of j. To illustrate, consider the example from Table 3.5 with $j = 2$ and eigenvalue $m = 0$. A larger graph is given in Fig. 3.9. From Fig. 3.9(A) it can be seen that the product of standard deviations predicts values of uncertainty similar to that of $j = 1/2$, Fig. 3.4(A). Yet when it comes to making a quantum mechanical prediction, the more complete Schrödinger uncertainty relation, Fig. 3.9(C), gives values of uncertainty when the Robertson relationship, Fig. 3.9(B), actually gives *no* uncertainty. For this state of $\mathbf{J}^{(2)}$ the standard Robertson uncertainty relation misses all uncertainty in every direction. So in this situation the Schrödinger relation raises the lower bound of uncertainty, though it does not bring the inequality of the uncertainty relation to an equality.

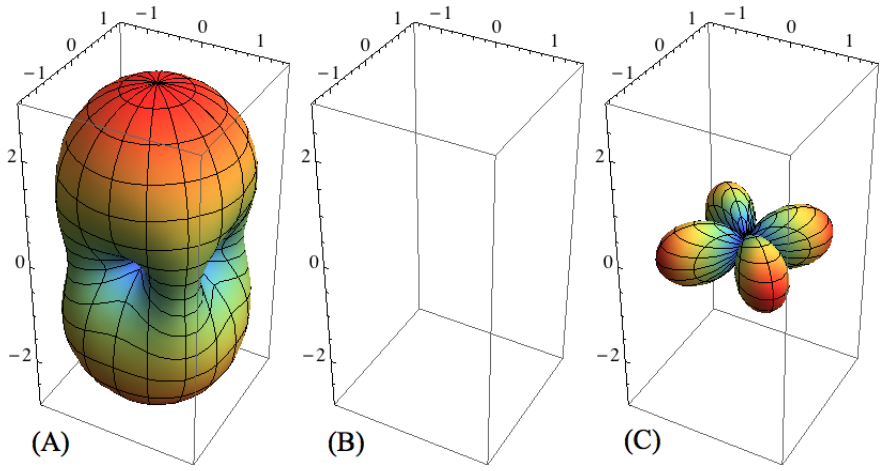

Figure 3.9 The magnitude of uncertainty for the orbital angular momentum eigenvectors of $\mathbf{J}^{(2)}$. $(A) = \sigma_{J_x^{(2)}}\sigma_{J_y^{(2)}}$, $(B) = \frac{1}{2i}\Big(\langle[J_x^{(2)}, J_y^{(2)}]\rangle\Big)$, $(C) = \sqrt{\Big(\frac{1}{2}\langle\{J_x^{(2)}, J_y^{(2)}\}\rangle - \langle J_x^{(2)}\rangle\langle J_y^{(2)}\rangle\Big)^2 + \Big(\frac{1}{2i}\langle[J_x^{(2)}, J_y^{(2)}]\rangle\Big)^2}$. These are plotted in spherical coordinates (θ, ϕ) with the amount of uncertainty in any particular direction corresponding to the value shown by the graph in that direction. Graph (A) corresponds to the multiplication of two standard deviations. The Robertson uncertainty relation (B) is zero. The Schrödinger uncertainty relation (C), captures some of the uncertainty for the generalized eigenvectors.

Chapter 4

Fidelity Analysis

4.1 Quantum Gate Fidelity Derivation

4.1.1 Quantum Gates

Traditional computers function using sophisticated electronic circuits that perform logic operations: the circuits move information around and the logic gates manipulate the information. Similarly, a quantum circuit contains channels through which information flows and quantum logic gates that manipulate the quantum information [18]. For example, the NOT gate has the following operation on the incoming information represented by zeros and ones:

$$0 \to 1 \qquad \text{and} \qquad 1 \to 0\,.$$

Thus the NOT gate interchanges the zeros for ones and vice versa. The analogous quantum NOT gate performs the operation

$$\alpha|0\rangle + \beta|1\rangle \to \alpha|1\rangle + \beta|0\rangle\,, \tag{4.1}$$

where $|0\rangle$ and $|1\rangle$ represent orthonormal basis states in the quantum space.

The action of quantum logic gates can be represented using matrix algebra, which is the formulation that I use throughout this chapter in dealing with quantum gate fidelity. For example, the quantum NOT gate operation shown in Eq. (4.1) can be represented in matrix form by writing the state $\alpha|0\rangle + \beta|1\rangle$ as

$$\begin{pmatrix} \alpha \\ \beta \end{pmatrix},$$

and the necessary matrix multiplication is given by

$$\begin{pmatrix} 0 & 1 \\ 1 & 0 \end{pmatrix}\begin{pmatrix} \alpha \\ \beta \end{pmatrix} = \begin{pmatrix} \beta \\ \alpha \end{pmatrix}. \tag{4.2}$$

The only constraint on the gate matrix, as in the two-by-two matrix in Eq. (4.2), is that a gate must be unitary. A unitary matrix U has the property $U^\dagger U = I$, where I is the identity.[1]

Besides representing logic gates as matrices, one can also represent the action of single-qubit logic gates on the Bloch sphere, which I utilize in the remaining chapters. As an illustrative example, the action of the non-trivial Hadamard gate

$$U_{Hadamard} = \frac{1}{\sqrt{2}}\begin{pmatrix} 1 & 1 \\ 1 & -1 \end{pmatrix}$$

on the normalized state

$$\frac{1}{\sqrt{2}}\big(|0\rangle + |1\rangle\big) = \frac{1}{\sqrt{2}}\begin{pmatrix} 1 \\ 1 \end{pmatrix}$$

is depicted in Fig. 4.1 with the corresponding matrix multiplication

$$\frac{1}{\sqrt{2}}\begin{pmatrix} 1 & 1 \\ 1 & -1 \end{pmatrix}\frac{1}{\sqrt{2}}\begin{pmatrix} 1 \\ 1 \end{pmatrix} = \begin{pmatrix} 1 \\ 0 \end{pmatrix}.$$

Any single qubit gate can be found by specifying two angles (θ, ϕ) in the arbitrary

[1] From this point onward I follow the convention in the quantum computation literature of dropping the hat (ˆ) above operators to simplify the notation and calculations.

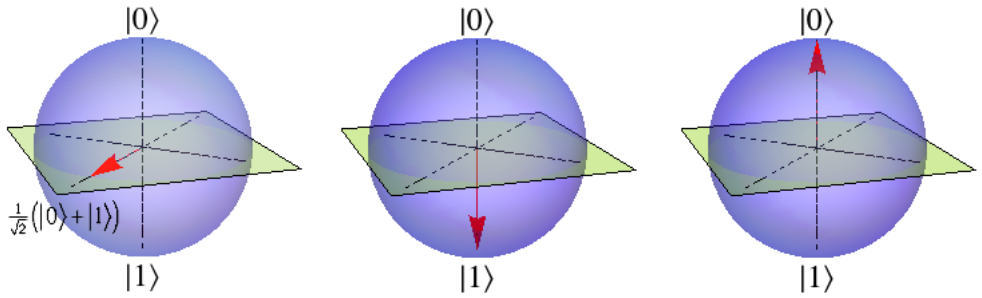

Figure 4.1 Visualization of the Hadamard gate acting on the state $\frac{1}{\sqrt{2}}\big(|0\rangle+|1\rangle\big)$. Beginning with the state in the $\hat{x}$–$\hat{y}$ plane, the gate rotates the state 90° and then reflects it through the $\hat{x}$–$\hat{y}$ plane.

single-qubit gate given by $U = e^{i\phi}\big(\cos(\theta/2)I + i\sin(\theta/2)\vec{u}\cdot\vec{\sigma}\big)$, where I is the identity, $\vec{u}$ is an arbitrary unit vector specified by two independent parameters, and $\vec{\sigma}$ is the Pauli matrix vector $\vec{\sigma} = (\sigma_x, \sigma_y, \sigma_z)$. I use this arbitrary single-qubit gate in my derivations and results on fidelity later in this chapter.

4.1.2 Gate Fidelity

As quantum states dynamically undergo evolutions in the process of computations, they will inevitably encounter some noise. Quantum states live somewhat frail lives, and the only way to absolutely ensure that no noise or decoherence is introduced into the state is to seal the state off from the rest of the universe. That is of course impossible and would defeat the whole point of performing a quantum computation: one needs the state to interact with something else to calculate anything. So a delicate balance must be maintained and the inevitable errors must be dealt with.

Gate fidelity is essentially a measure of how successfully a gate has preserved a state from acquiring noise. For example, if as part of a quantum computation I wish to implement a particular gate U, then I am assured that it was not exactly U that was implemented, but a noisy version called $\mathcal{E}$. By calculating the gate fidelity I

can know how successful U has been in keeping noise out of the state $|\psi\rangle$. The gate fidelity F essentially keeps track of the difference between what really happened in the computation and what was intended to happen; it is defined as

$$F(U,\mathcal{E}) \equiv \min_{|\psi\rangle} F\Big(U|\psi\rangle, \mathcal{E}(|\psi\rangle\langle\psi|)\Big) = \mathrm{Tr}\sqrt{\rho^{1/2}\sigma\rho^{1/2}} \tag{4.3}$$

which is essentially the overlap of the two mixed states ρ and σ, and where $\min_{|\psi\rangle}$ indicates that the minimum over $|\psi\rangle$ is to be taken.

4.2 Conservation Laws and Gate Fidelity

In addition to the customary decoherence that creeps in through environmental and controller-induced factors, recent work [5] suggests that conservation laws limit the accuracy of quantum gate operations. The Wigner-Araki-Yanase theorem shows that conservation laws limit the accuracy of a quantum measurement [25, 26]. This theorem has been generalized to show that conservation laws also limit the accuracy of quantum gates [27]. The inherent errors that arise due to conflicts with angular momentum conservation laws have been evaluated for some specific gates [27] and findings were recently reported on the nature of arbitrary single-qubit gates [5]. This thesis builds upon the arbitrary single-qubit case by applying the Schrödinger uncertainty relation.

In this section I will connect conservation laws to gate fidelity, Eq. (4.3). Following the assumption made in the Wigner-Araki-Yanase theorem, I assume that there exists additive conserved quantities L_S and L_A of the system (S) and ancilla[2] (A) such that

$$L = L_S \otimes I_A + I_S \otimes L_A \tag{4.4}$$

[2]An ancilla is often used as an extra quantum system that is cast aside after it has fulfilled its particular purpose.

where I_S and I_A are the identity operators of system and ancilla respectively. I further assume that for the additive conserved quantity L and for a unitary operator U the conservation law

$$[U, L] = 0 \tag{4.5}$$

must be satisfied. Our U here is arbitrary and corresponds only to what satisfies the conservation law Eq. (4.5). Eq. (4.5) is an example of the familiar tenet of quantum theory that when an operator commutes with the Hamiltonian it is a constant of the motion, i.e., that operator gives rise to a conserved quantity. In the present case however, U represents a unitary quantum gate.

According to the Wigner-Araki-Yanase theorem [26], (hereafter abbreviated as WAY), any operator $\mathcal{O}$ which does not commute with an additive conserved quantity (such as L from above) will impose a limitation on the measurement of that operator. Thus the WAY theorem states: given the operator $\mathcal{O}$ and that the conservation law $[U, L] = 0$ is satisfied, if $[\mathcal{O}, L] \neq 0$ then a von Neumann measurement of $\mathcal{O}$ is not possible. In this paper I am concerned with a generalization of this theorem in which the additive conserved quantity imposes a limitation on quantum gates.

In order to connect the WAY theorem with quantum gate fidelity we make use of the deviation operator D from [5] for a system and ancilla. This deviation operator originates from a particular measurement theory formulated by M. Ozawa [28] and effectively represents the difference between two transformations. The deviation operator can be defined as

$$D = U^{\dagger}(L_S \otimes I_A)U - U_S^{\dagger} L_S U_S \otimes I_A. \tag{4.6}$$

From previous analysis [5] we use the following parameterizations for the pieces of Eq. (4.6): $L_S = c\,\vec{l}\cdot\vec{\sigma}$ where c is the eigenvalue of L_S, $\vec{l}$ is an arbitrary unit vector, $\vec{\sigma}$ is the Pauli matrix vector $\vec{\sigma} = (\sigma_x, \sigma_y, \sigma_z)$, U_S is an arbitrary single-qubit gate given

by $U_S = e^{i\phi}\big(\cos(\theta/2)I_S + i\sin(\theta/2)\vec{u}\cdot\vec{\sigma}\big)$, $\vec{u}$ is an arbitrary unit vector, and $U_S^\dagger$ is the conjugate transpose of U_S.

It can be shown using $[U, L] = 0$, Eq. (4.4), and Eq. (4.6) that $[D, L] \neq 0$. Thus by the WAY theorem D cannot be measured completely. Using this fact, Karasawa et al. [5] developed a relation between the mean square $\langle D^2\rangle$ and fidelity which is expressed as

$$\langle D^2\rangle \leq 4c^2(1 - F(\mathcal{E}, U_S)^2) \tag{4.7}$$

where the fidelity $F(\mathcal{E}, U_S)$ of the trace preserving quantum channel $\mathcal{E}$ is measured relative to the arbitrary single-qubit gate U_S and where c is an eigenvalue of L_S. The standard deviation of D gives a lower bound of the fidelity. I observe that $\sigma_D^2 = \langle D^2\rangle - \langle D\rangle^2 \leq \langle D^2\rangle$ and from (4.7) I have

$$\sigma_D^2 \leq 4c^2(1 - F(\mathcal{E}, U_S)^2)\,. \tag{4.8}$$

This result can be used to introduce the Schrödinger uncertainty relation.

4.3 Fidelity Employing the Schrödinger Uncertainty Relation

Since $[D, L] \neq 0$, the operators D and L are incompatible observables and thus an uncertainty relation can be defined between them. Previous work [5, 27, 28] used the Robertson uncertainty relation

$$\sigma_A^2\sigma_B^2 \geq \Big(\frac{1}{2i}\langle[A, B]\rangle\Big)^2\,. \tag{4.9}$$

However, as illustrated throughout this thesis, the Schrödinger uncertainty relation given by

$$\sigma_A^2\sigma_B^2 \geq \Big(\frac{1}{2}\langle\{A, B\}\rangle - \langle A\rangle\langle B\rangle\Big)^2 + \Big(\frac{1}{2i}\langle[A, B]\rangle\Big)^2\,, \tag{4.10}$$

is often more complete and would give a fuller picture of the constraints on gate operations due to conservation laws.

I now connect the Schrödinger uncertainty relation to fidelity using the incompatible observables D and L. In order to develop the uncertainty relation in the most applicable way, I consider the case of mixed states. From Chapter 2, I know that the Schrödinger uncertainty relation can be expressed in terms of mixed states and the operators D and L as

$$\sigma_D^2\sigma_L^2 \geq \Big(\frac{1}{2}Tr(\rho\{D,L\}) - Tr(\rho D)Tr(\rho L)\Big)^2 + \Big(\frac{1}{2i}Tr(\rho[D,L])\Big)^2 \tag{4.11}$$

where ρ is an arbitrary mixed state of the form $\rho = \frac{1}{2}(I + \vec{u}\cdot\vec{\sigma})$ and where I is the identity. Solving for σ_D^2 I have simply

$$\sigma_D^2 \geq \frac{1}{\sigma_L^2}\left[\Big(\frac{1}{2}Tr(\rho\{D,L\}) - Tr(\rho D)Tr(\rho L)\Big)^2 + \Big(\frac{1}{2i}Tr(\rho[D,L])\Big)^2\right]. \tag{4.12}$$

From the relationship between the deviation operator and fidelity (4.8), I solve for the fidelity to get

$$\sqrt{1 - \frac{1}{4c^2}\sigma_D^2} \geq F(\mathcal{E}, U_S). \tag{4.13}$$

where σ_D^2 is Eq. (4.12). The best case scenario is when this relation is an equality,

$$F(\mathcal{E}, U_S) = \sqrt{1 - \frac{1}{4c^2}\sigma_D^2} \tag{4.14}$$

which is the fidelity in terms of the Schrödinger uncertainty relation. For comparison, in Chapter 5 I will use both Eq. (4.14) and a version with the Robertson relation inserted into the equation instead of the Schrödinger relation.

Chapter 5

Fidelity Data

5.1 Calculating Fidelity

My principal goal in calculating fidelity using the Schrödinger relation is to show that the Schrödinger relation restricts fidelity more than the Robertson relation does. As discussed in Section 2.4, the Schrödinger contributions either add some positive real value to the uncertainty, or they add nothing, and more often than not, the additions are nonzero.

However, actually carrying out the computations for the Schrödinger version of fidelity is a difficult task and one that I have only been able to perform by making many approximations. In this section I discuss these approximations and the results of the calculations. I wish to emphasize that because of the approximations, I do not make definitive claims, such as ruling out certain quantum gates from being realizable in the lab because their fidelity is too low; rather, my results suggest that the Schrödinger relation imposes greater and more accurate restrictions that should be addressed more completely in future research.

Challenges arise when computing the fidelity in Eq. (4.14). If I leave the expres-

sion completely general, (allowing for the operators to have complex matrix entries) then there are up to 49 independent parameters that must be taken into account. Judiciously picking parameters by imposing some constraints could trim this number down. After making some assumptions (detailed in the next few paragraphs) and taking into account all the definitions discussed in Section 4.2, I cut down the number of independent parameters to 9. The 9 parameters include the following: 4 parameters for the generalized gate U_S, 2 parameters for the state (a density operator), 2 parameters for the operator L_S, and 1 parameter for the eigenvalue c. All of this comes to a grand total of 9 independent parameters that must be specified in the calculations.

The unitary matrix U accounts for 32 of the 49 parameters. In the paper that I primarily use for connecting fidelity to uncertainty, Karasawa et al. [5] never specify U because in finding the commutator $[D, L] = -[U_S^\dagger L_S U_S, L_S] \otimes I_A$, U cancels out. However, the anticommutator $\{D, L\}$ works out to

$$\begin{aligned}\{D, L\} =& 2\Big((U^\dagger L_S \otimes I_A U)(L_S \otimes I_A) + (U^\dagger L_S \otimes I_A U)(I_S \otimes L_A) \\ & - (U_S^\dagger L_S U_S \otimes I_A)(I_S \otimes L_A)\Big) - \{U_S^\dagger L_S U_S, L_S\} \otimes I_A. \end{aligned} \tag{5.1}$$

Clearly, U does not cancel out in this case. Since the Schrödinger uncertainty relation contains an anticommutator, it is thus necessary to either specify a U and thereby cut out 32 parameters or keep U general and compute with all 32. In Section 5.2 I specify and compare three different U's in calculating fidelity; but not only do I specify the U's, but I approximate the general four-by-four U matrix with single-qubit gates that are two-by-two matrices (I will later discuss more simplifications that make the dimensions work out).

Furthermore, I assume that I am working with a spin-like system with eigenvalue $c = 1/2$. I assume that since L_A is only the conserved quantity of the ancilla and not of the system, the total $L = L_S \otimes I_A + I_S \otimes L_A$ can be approximated by $L = L_S$, which

also cuts the dimensions of L down from four to two.[1] To make the dimensions work out, I also assume that I_S and I_A can be ignored. Next, I assume that $\sigma_L^2 = 1$ because the division necessary to compute Eq. (5.3) makes the computations longer but does not change the qualitative nature of the results; the primary result that I am after in this thesis is to show that the Schrödinger relation raises the lower bound on fidelity in comparison to the Robertson relation. Since I leave out the division by σ_L^2 in *both* the Robertson and Schrödinger cases, the relative difference between the two remains the same; division by σ_L^2 just acts like a factor that scales both relations and does not matter when I look at the difference between the two relations.

I can also employ a simplification used by Karasawa et al. [5] by observing that since I am interested in the worst case error, I need not calculate expectation values but rather take the supremum for any operator X as follows:

$$\sup_{|\psi\rangle} |\langle X \rangle| = \|X\|, \tag{5.2}$$

where $\|X\|$ is the operator norm of X. Since X in the present context is a matrix, the operator norm $\|X\|$ is defined as the square root of the largest eigenvalue of the symmetric matrix $X^T X$, where ^{T} denotes the transpose. Thus when I calculate fidelity, Eq. (4.12) becomes

$$\sigma_D^2 \geq \frac{1}{\sigma_L^2}\left[\left(\frac{1}{2}\|\{D, L\}\| - \big(\|D\|\big)\big(\|L\|\big)\right)^2 + \left(\frac{1}{2i}\|[D, L]\|\right)^2\right]. \tag{5.3}$$

This assumption cuts the 9 parameters down to 7; in the next section I use two methods of calculation, one that uses 9 parameters and another that uses 7. With all of these assumptions and simplifications in hand that cut the independent parameters down from 49 to 9 or 7, I am ready to compute the fidelity in Eq. (4.14).

[1] One possible issue with this assumption is that because I drop so many degrees of freedom in L, it is possible that the condition for the WAY theorem $[U, L] = 0$ may not be satisfied depending on the parameterization of U. The parameter values I choose for the figures later in the chapter ensure that 2 of the 3 different U's satisfy the commutation relation $[U, L_S] = 0$.

5.2 Fidelity in Three Specific Cases

My goals in calculating fidelity for arbitrary single-qubit gates are first to show that the Schrödinger relation drops the upper bound on fidelity and then to propose the process as a computational feasibility check that would set an upper bound on fidelity for certain quantum computations. Depending on the quantum computer and task at hand, the required fidelity varies. For various tasks and sets of assumptions about the quantum computing architecture, the required fidelity ranges from minima such as 0.95 [29] to 0.99 and higher for some tasks [30]. Accordingly, one can know *a priori* if a certain quantum computation will be feasible by doing some preliminary fidelity calculations. The results of this section suggest that conservation law constraints may actually exclude many quantum computational processes.

To illustrate that the Schrödinger relation raises the lower bound and that my calculations constitute a rough feasibility check, in this section I present two methods of calculating the fidelity: (1) I calculate the fidelity using the assumption discussed in the paragraph surrounding Eq. (5.2), and (2) I calculate the fidelity by taking the expectation value (using mixed states) implied by the uncertainty relations. For both methods, I compare the three scenarios (1) when U is the Hadamard gate, (2) when U is the phase gate, and (3) when U is the $\pi/8$ gate, which are all defined as

$$U_{Hadamard} = \frac{1}{\sqrt{2}} \begin{pmatrix} 1 & 1 \\ 1 & -1 \end{pmatrix} \tag{5.4}$$

$$U_{phase} = \begin{pmatrix} 1 & 0 \\ 0 & i \end{pmatrix} \tag{5.5}$$

$$U_{\pi/8} = \begin{pmatrix} 1 & 0 \\ 0 & e^{i\pi/4} \end{pmatrix}. \tag{5.6}$$

I choose these three gates for U simply to illustrate some possibilities.[2]

Method (1) has the advantage that there are fewer parameters to specify, since I do not need two of the parameters that characterize the mixed state ρ. However, the operator norm in Eq. (5.2) is difficult to calculate for the commutator and anticommutator in Eq. (5.3) because the operators that result from multiplying out the commutator and anticommutator are quite complex; they consist of two-by-two matrices that are approximately 1/2 of a page of trigonometric functions in *Mathematica* code and the exact eigenvalues—needed to calculate the operator norm—are equally long, complex, and thus unenlightening. Consequently, I calculate the operator norm numerically—and hence approximately—for each of the operators individually in Eq. (5.3).

I calculate fidelity in method (1) by first inputing a range of numerical values into the large two-by-two matrices that represent the operators. These values are in the range of the parameters, e.g., θ has the range of values $0 \leq \theta \leq \pi$ in a certain step size. After inserting many values for all the independent parameters, I now have a large number of two-by-two matrices, which for clarity in the discussion here I call A_i. I take all the A_i matrices and calculate the operator norm of each one by taking the square root of the largest eigenvalue for all the symmetric matrices $A_i^T A_i$. I now compute the fidelity using these operator norm values.

The results of the calculations of fidelity for incrementally smaller step sizes is shown in Fig. 5.1. As the step size gets smaller, the fidelity for both the Robertson and Schrödinger uncertainty relations appears to roughly converge, with the Robertson relation consistently predicting a fidelity higher than that predicted by the Schrödinger relation. The data shown in Fig. 5.1 is discussed in more detail in Table 5.1, and the

[2]The parameter values I choose for Fig. 5.2 later in this section ensure that the phase gate and the $\pi/8$ gate satisfy the commutation relation $[U, L_S] = 0$.

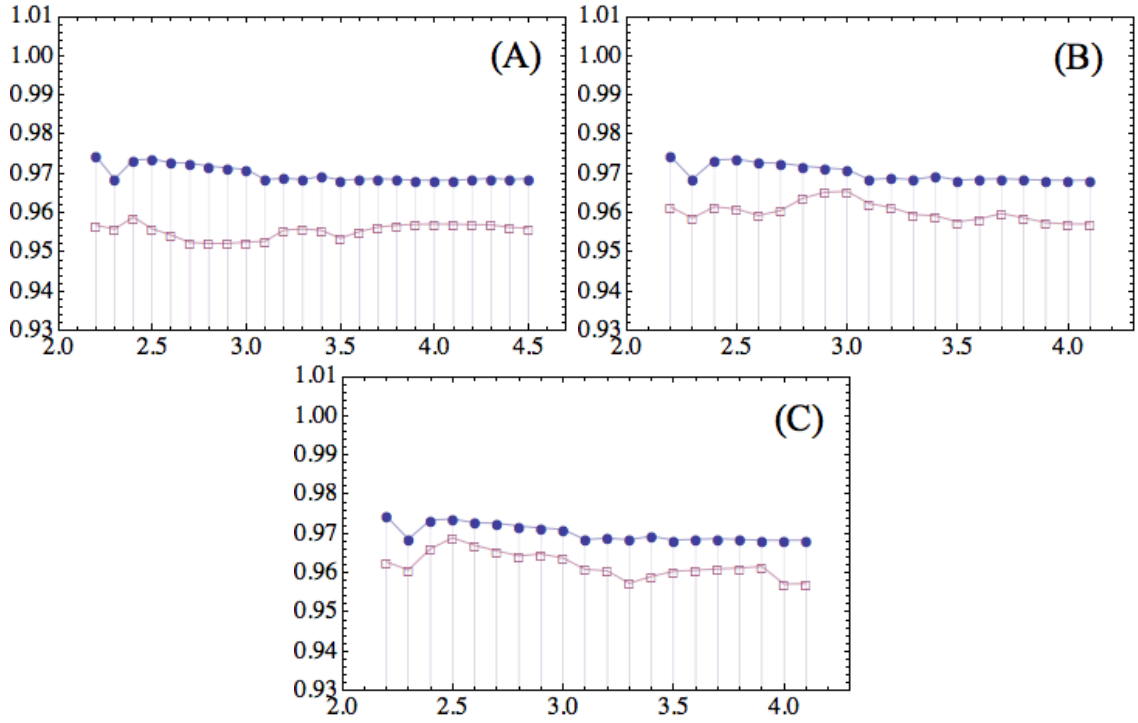

Figure 5.1 Gate fidelity numerical results. Fidelity (y-axis) is plotted as a function a parameter that is inversely proportional to the step size (x-axis). The fidelity data points for the Robertson relation are filled circles • and for the Schrödinger relation they are empty squares □. Lines are drawn down to the axis for reading convenience. (A) Comparing Robertson and Schrödinger versions of fidelity for when U is the Hadamard gate. (B) Comparing Robertson and Schrödinger versions of fidelity for when U is the phase gate. (C) Comparing Robertson and Schrödinger versions of fidelity for when U is the $\pi/8$ gate. In (A)-(C) it can be seen that fidelity using the Robertson relation is higher than fidelity using the Schrödinger relation.

Mathematica code for the computations is contained in Appendix C.

Method (2) of calculating fidelity has the advantage that no further assumptions, such as the supremum assumption in Eq. (5.2), are necessary. I simply compute Eq. (4.14) directly. Furthermore, the result is exact and can be depicted in the Bloch sphere (if values are given for all the parameters but two). The problem with this method, however, is that there are many parameters in the computations and the results (unlike method (1) which gives a single numeric answer). A result in terms of many parameters is difficult to decipher and tends to help little in practical and

Table 5.1 Numerical fidelity data, rounded to four significant figures. Comparison of the fidelity for two gates calculated using operator norms for both the Robertson and Schrödinger relations, as shown in Fig. 5.1. The standard deviation of the data is given under σ and under the "Difference" column are the differences between the mean values.

Gate U	Robertson Mean	σ	Schrödinger Mean	σ	Difference
Hadamard	0.9693	0.0017	0.9518	0.0034	0.0175
Phase	0.9702	0.0022	0.9603	0.0025	0.0100
$\pi/8$	0.9702	0.0022	0.9620	0.0033	0.0081

experimental situations—the experimenter or engineer has sufficiently many variables of equipment and method of execution to worry about without the added hassle of making sure they keep track of 9 independent parameters as well.

The results of method (2), calculating the fidelity in Eq. (4.14) directly and supplying values for all parameters except for two, are shown in Fig. 5.2. These particular plots are in the Bloch sphere representation in terms of the two parameters that specify the conserved quantity L. By analogy to the plots in Chapter 3, they represent the fidelity for the specific single-qubit gates given a conserved quantity that "points" in a particular direction on the Bloch sphere. The key result is that using the Schrödinger relation in fidelity further limits the maximum fidelity possible.

Though not shown here, I have also made dynamic plots of the results of the fidelity calculations using method (2); these dynamic plots allow me to vary all the parameters in terms of the others and the plots are the same in their essential features to those given in Fig. 5.2. The dynamic plots also give slightly deformed spheres and they deform somewhat irregularly, though never drastically, as all the parameters are varied. I am not certain if the very subtle deformations in the spheres as the parameters vary are meaningful or simply an artifact of the approximations I make. As far as I have been able to ascertain, no matter the deformations, the key result

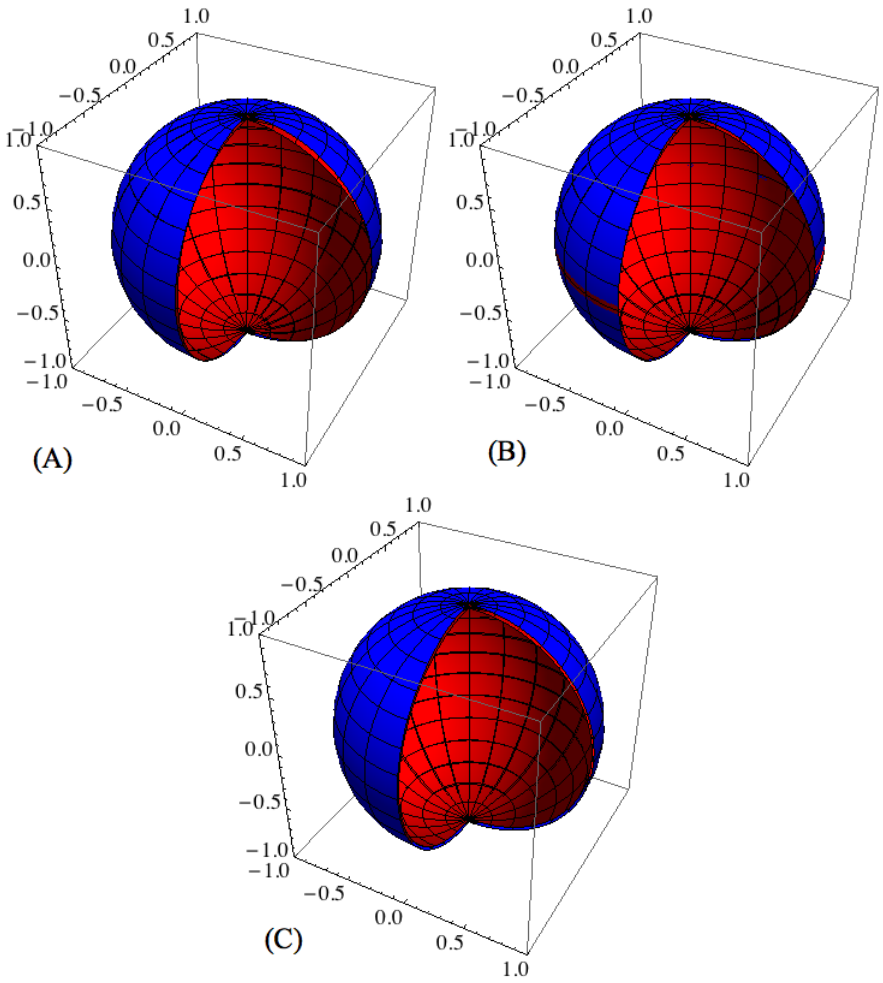

Figure 5.2 Bloch sphere gate fidelity. Plots of fidelity in the Bloch sphere in terms of the two parameters that specify the conserved quantity L, and where all the remaining parameters are given the value of zero. The blue outer spherical figures are for fidelity using the Robertson relation while the red inner spherical figures are for fidelity using the Schrödinger relation. A segment of all the figures has been removed to reveal the inner structure. The fidelity plots are for when U is (A) the Hadamard gate, (B) the phase gate, and (C) the $\pi/8$ gate. These plots show that the Schrödinger relation further limits the maximum fidelity possible because all the red Schrödinger spherical figure is contained inside the blue Robertson spherical figure, except for the phase gate near the "equator" and the Hadamard gate only *exactly* at the "equator" where both Robertson and Schrödinger have a value of 1. In general, both the red and the blue spherical figures slightly deform (remaining near 1) as the parameters change. For these particular plots where all the parameters besides those for L are set to zero, the Robertson fidelity is always 1, i.e., the Robertson plot is a unit sphere. Values of fidelity of the Schrödinger spheres with the azimuthal angle (corresponding to ϕ in Fig. 1.2.2) set to zero and at various values of the polar angle (corresponding to θ in Fig. 1.2.2) as measured down from the $\hat{z}$ axis: at 0° (A)=(B)=(C)=0.9682; at 45° (A)=0.9682, (B)=0.9922, (C)=0.9770; and at 90° (A)=1, (B)=1, (C)=0.9843.

persists that the Schrödinger fidelity almost always remains smaller—and hence more restrictive—than the Robertson fidelity.

5.3 Discussion of Fidelity Data

The most important result in this chapter is that using the Schrödinger relation in fidelity further limits the maximum fidelity possible for certain single-qubit gates, given the presence of a conserved quantity. Both methods that I employ in calculating fidelity arrive at this same conclusion and suggest that conservation law constraints may exclude many computations *a priori*. However, the process of finding the fidelity restrictions is somewhat messy because so many parameters are involved. In both methods I have had to make some simplifying assumptions that render the final results less general than I would like. Therefore I am not confident enough in the results to make detailed claims. For example, I cannot use the data from Fig. 5.1 to propose that all single-qubit gates in the presence of a conserved quantity are restricted from achieving fidelities of 0.99—as would be necessary for many computations [30]. I do think, however, that my results are highly suggestive of possible restrictions and that researchers should seriously consider conservation law constraints.

Further research on this topic could simplify the calculations, or perhaps more significantly, adjust some of the underlying theory so that results can be more readily usable for experimental applications. Ideally these modifications would result in fewer parameters and greater accuracy in foreseeing which computations may be unfeasible.

Chapter 6

Conclusions

In Chapters 2 and 3 of this thesis, I have discussed the nature of the Schrödinger uncertainty relation for pure and mixed states. I have illustrated the discrepancies between the Robertson and Schrödinger uncertainty relations, showing that in many cases the Schrödinger uncertainty relation raises the lower bound on uncertainty. I conclude that in situations where quantum uncertainty must be accounted for, researchers should utilize the Schrödinger uncertainty relation.

In Chapters 4 and 5, I applied the Schrödinger uncertainty relation to quantum gate fidelity and discussed two computational processes which attempt to place an upper bound on fidelity for certain computational systems. These methods should be seen as a possible feasibility check; by following these methods one can know *a priori* if a certain quantum computation will be feasible or not. Though my final results are less general than I would like, they are nonetheless highly suggestive of significant fundamental restrictions and of the role that the Schrödinger uncertainty relation has in more accurately predicting such restrictions.

Appendix A

Angular Momentum Matrices

In this appendix I write out explicitly the angular momentum matrices $\mathbf{J}_r^{(1/2)}, \mathbf{J}_r^{(1)}$, $\mathbf{J}_r^{(3/2)}$, and $\mathbf{J}_r^{(2)}$, which represent the angular momentum for an arbitrary direction $\hat{r}$ in the J^2, J_z basis. These matrices are derived according to the method in Section 3.3.1. The matrices $J_i^{(1)}, J_i^{(3/2)}$, and $J_i^{(2)}$, where $i = x, y, z$, are necessary for deriving $\mathbf{J}_r^{(1)}$, $\mathbf{J}_r^{(3/2)}$, and $\mathbf{J}_r^{(2)}$. The derivation of the matrices $J_i^{(1)}, J_i^{(3/2)}$, and $J_i^{(2)}$ is discussed in [31], pgs. 504-508. The matrix $\mathbf{J}_r^{(1/2)}$ has eigenvalues of $\pm\hbar/2$. The matrix $\mathbf{J}_r^{(1)}$ has eigenvalues of 0 and $\pm\hbar$, the matrix $\mathbf{J}_r^{(3/2)}$ has eigenvalues of $\pm\hbar/2$ and $\pm 3\hbar/2$, and the matrix $\mathbf{J}_r^{(2)}$ has eigenvalues of 0, $\pm\hbar$ and $\pm 2\hbar$

$$\mathbf{J}_r^{(1/2)} = \frac{\hbar}{2}\begin{pmatrix} \cos\theta & e^{-i\phi}\sin\theta \\ e^{i\phi}\sin\theta & -\cos\theta \end{pmatrix} \tag{A.1}$$

$$\mathbf{J}_r^{(1)} = \frac{\hbar}{\sqrt{2}}\begin{pmatrix} \sqrt{2}\cos\theta & \sin\theta e^{-i\phi} & 0 \\ \sin\theta e^{i\phi} & 0 & \sin\theta e^{-i\phi} \\ 0 & \sin\theta e^{i\phi} & -\sqrt{2}\cos\theta \end{pmatrix} \tag{A.2}$$

$$\mathbf{J}_r^{(3/2)} = \hbar \begin{pmatrix} \frac{3}{2}\cos\theta & \frac{\sqrt{3}}{2}\sin\theta e^{-i\phi} & 0 & 0 \\ \frac{\sqrt{3}}{2}\sin\theta e^{i\phi} & \frac{1}{2}\cos(\theta) & \sin\theta e^{-i\phi} & 0 \\ 0 & \sin\theta e^{i\phi} & -\frac{1}{2}\cos\theta & \frac{\sqrt{3}}{2}\sin\theta e^{-i\phi} \\ 0 & 0 & \frac{\sqrt{3}}{2}\sin\theta e^{i\phi} & -\frac{3}{2}\cos\theta \end{pmatrix} \tag{A.3}$$

$$\mathbf{J}_r^{(2)} = \hbar \begin{pmatrix} 2\cos(\theta) & \sin(\theta)e^{-i\phi} & 0 & 0 & 0 \\ \sin(\theta)e^{i\phi} & \cos(\theta) & \frac{\sqrt{6}}{2}\sin(\theta)e^{-i\phi} & 0 & 0 \\ 0 & \frac{\sqrt{6}}{2}\sin(\theta)e^{i\phi} & 0 & \frac{\sqrt{6}}{2}\sin(\theta)e^{-i\phi} & 0 \\ 0 & 0 & \frac{\sqrt{6}}{2}\sin(\theta)e^{i\phi} & -\cos(\theta) & \sin(\theta)e^{-i\phi} \\ 0 & 0 & 0 & \sin(\theta)e^{i\phi} & -2\cos(\theta) \end{pmatrix} \tag{A.4}$$

Appendix B

Mathematica Code for Numerical Spin Eigenvalues and Eigenvectors

Because the eigenvectors of the matrices $\mathbf{J}_r^{(1)}$, $\mathbf{J}_r^{(3/2)}$, and $\mathbf{J}_r^{(2)}$, are quite complex, I find it most convenient to calculate and use their eigenvectors numerically for calculating uncertainties in the case of $j = 1, 3/2, 2$. What follows is the *Mathematica* code that I used to numerically calculate and plot the uncertainties. I have included notes in the code by using the method of including notes in *Mathematica*, denoted by the symbols (* *) to surround the notes. In all my calculations I have set $\hbar = 1$.

B.1 Code for $\mathbf{J}_r^{(1)}$

The following is the code for calculating $\sigma_{J_x^{(1)}}\sigma_{J_y^{(1)}}$.

```
Clear["`*"]
h = 25; (*step size*)m = 20;(*plot points*)

(*This matrix "M" corresponds to l=1*)
M = (1/Sqrt[2])*{{Sqrt[2]*Cos[\[Theta]], Sin[\[Theta]]*E^(-I*\[Phi]),0},
{Sin[\[Theta]]*E^(I*\[Phi]), 0, Sin[\[Theta]]*E^(-I*\[Phi])},
```

```
{0, Sin[\[Theta]]*E^(I*\[Phi]), -Sqrt[2]*Cos[\[Theta]]}};

(*Makes the matrix M numeric*)
Flatten[Table[M, {\[Theta], 0.0, Pi, Pi/h}, {\[Phi], 0.0, 2*Pi, 2*Pi/h}], 1];
eigen = Chop[Map[Eigenvectors, %]];
dim = Dimensions[eigen];
normalizedVectors = Map[Normalize, eigen, {2}];

(*The eigenvectors with corresponding eigenvalues for +-1 are {1} and {2},
while it is 0 for {3}*)
secondVectors = Take[normalizedVectors, All, {1}];

\[Psi]\[Dagger] = Map[Conjugate, secondVectors];
\[Psi] = Map[ConjugateTranspose, \[Psi]\[Dagger]];
Table[\[Psi]\[Dagger][[i]].\[Psi][[i]], {i, 1, dim[[1]]}];
Flatten[%, 2]; (*This is a big list of values, in a long vector form*)

\[CapitalLambda]x = {{0, (1/Sqrt[2]), 0}, {(1/Sqrt[2]), 0, (1/Sqrt[2])}, {0, (1/Sqrt[2]), 0}};
\[CapitalLambda]x2 = \[CapitalLambda]x.\[CapitalLambda]x;

Lx =  Table[\[Psi]\[Dagger][[i]].\[CapitalLambda]x.\[Psi][[i]], {i, 1, dim[[1]]}];
Lx2 = Table[\[Psi]\[Dagger][[i]].\[CapitalLambda]x2.\[Psi][[i]], {i, 1, dim[[1]]}];

\[CapitalLambda]y ={{0, -I*(1/Sqrt[2]),0}, {I*(1/Sqrt[2]), 0, -I*(1/Sqrt[2])}, {0, I*(1/Sqrt[2]), 0}};
\[CapitalLambda]y2 = \[CapitalLambda]y.\[CapitalLambda]y;

Ly = Table[\[Psi]\[Dagger][[i]].\[CapitalLambda]y.\[Psi][[i]], {i, 1,dim[[1]]}];
Ly2 = Table[\[Psi]\[Dagger][[i]].\[CapitalLambda]y2.\[Psi][[i]], {i,1, dim[[1]]}];

\[CapitalDelta]Lx = Sqrt[Lx2 - Lx^2];
\[CapitalDelta]Ly = Sqrt[Ly2 - Ly^2];

LHS = Flatten[\[CapitalDelta]Lx*\[CapitalDelta]Ly, 2];
dir[theta_, phi_] := {Sin[theta]*Cos[phi], Sin[theta]*Sin[phi],Cos[theta]}
sphereValues =Flatten[Table[dir[\[Theta], \[Phi]], {\[Theta], 0.0, Pi, Pi/h},
{\[Phi], 0.0,2*Pi, 2*Pi/h}], 1];

(*This is a three-dimensional plot of the uncertainty*)
ListSurfacePlot3D[Chop[sphereValues*LHS], MaxPlotPoints -> m]
```

The following code is for calculating the Robertson and Schrödinger uncertainties, for $J_x^{(1)}$ and $J_y^{(1)}$.

```
Clear["*`"]
h = 30; (*step size*)m = 20;(*plot points*)

M = (1/Sqrt[2])*{{Sqrt[2]*Cos[\[Theta]], Sin[\[Theta]]*E^(-I*\[Phi]),0},
{Sin[\[Theta]]*E^(I*\[Phi]), 0, Sin[\[Theta]]*E^(-I*\[Phi])},
{0, Sin[\[Theta]]*E^(I*\[Phi]), -Sqrt[2]*Cos[\[Theta]]}};

Flatten[Table[M, {\[Theta], 0.0, Pi, Pi/h}, {\[Phi], 0.0, 2*Pi, 2*Pi/h}], 1];
eigen = Chop[Map[Eigenvectors, %]];
dim = Dimensions[eigen];
normalizedVectors = Map[Normalize, eigen, {2}];

secondVectors = Take[normalizedVectors,All, {1}];
(*Change which eigenvectors to use here->{?}*)
(*eigenvalue +-1 is {1,2}; eigenvalue 0 is {3}*)

\[Psi]\[Dagger] = Map[Conjugate, secondVectors];
\[Psi] = Map[ConjugateTranspose, \[Psi]\[Dagger]];
Table[\[Psi]\[Dagger][[i]].\[Psi][[i]], {i, 1, dim[[1]]}];
Flatten[%, 2]; (*This is a big list of values, in a long vector form*)

\[CapitalLambda]x ={{0, (1/Sqrt[2]), 0}, {(1/Sqrt[2]),0, (1/Sqrt[2])}, {0, (1/Sqrt[2]), 0}};
Lx =  Table[\[Psi]\[Dagger][[i]].\[CapitalLambda]x.\[Psi][[i]], {i, 1,dim[[1]]}];
\[CapitalLambda]y ={{0, -I*(1/Sqrt[2]),0}, {I*(1/Sqrt[2]), 0, -I*(1/Sqrt[2])}, {0, I*(1/Sqrt[2]), 0}};

Ly = Table[\[Psi]\[Dagger][[i]].\[CapitalLambda]y.\[Psi][[i]], {i, 1,dim[[1]]}];
\[CapitalLambda]x\[CapitalLambda]y = \[CapitalLambda]x.\[CapitalLambda]y;

LxLy = Table[\[Psi]\[Dagger][[i]].\[CapitalLambda]x\[CapitalLambda]y.\[Psi][[i]], {i,1,dim[[1]]}];
\[CapitalLambda]y\[CapitalLambda]x = \[CapitalLambda]y.\[CapitalLambda]x;
LyLx = Table[\[Psi]\[Dagger][[i]].\[CapitalLambda]y\[CapitalLambda]x.\[Psi][[i]], {i,1, dim[[1]]}];

Com = LxLy - LyLx;
ACom = LxLy + LyLx;

Robertson = Flatten[Sqrt[(1/(2*I)*Com)^2], 2];
```

```
Schrodinger = Flatten[Sqrt[(1/2*ACom - Lx*Ly)^2 + (1/(2*I)*Com)^2], 2];

dir[theta_, phi_] := {Sin[theta]*Cos[phi], Sin[theta]*Sin[phi],Cos[theta]}
sphereValues = Flatten[Table[dir[\[Theta], \[Phi]], {\[Theta], 0.0, Pi, Pi/h},
{\[Phi], 0.0,2*Pi, 2*Pi/h}], 1];

ListSurfacePlot3D[Chop[sphereValues*Robertson], MaxPlotPoints -> m]

ListSurfacePlot3D[Chop[sphereValues*Schrodinger], MaxPlotPoints -> m]
```

B.2 Code for $\mathbf{J}_r^{(3/2)}$

The following is the code for calculating $\sigma_{J_x^{(3/2)}}\sigma_{J_y^{(3/2)}}$.

```
Clear["`*"]
h = 30; (*step size*)m = 22;(*plot points*)

M ={{3/2 Cos[\[Theta]],Sqrt[3]/2 Sin[\[Theta]]*E^(-I*\[Phi]), 0, 0},
{Sqrt[3]/2 Sin[\[Theta]]*E^(I*\[Phi]), 1/2 Cos[\[Theta]],Sin[\[Theta]]*E^(-I*\[Phi]), 0},
{0, Sin[\[Theta]]*E^(I*\[Phi]), -1/2*Cos[\[Theta]], Sqrt[3]/2 Sin[\[Theta]]*E^(-I*\[Phi])},
{0, 0, Sqrt[3]/2 Sin[\[Theta]]*E^(I*\[Phi]), -3/2 Cos[\[Theta]]}};

Flatten[Table[M, {\[Theta], 0.0, Pi, Pi/h}, {\[Phi], 0.0, 2*Pi, 2*Pi/h}], 1];
eigen = Chop[Map[Eigenvectors, %]];
dim = Dimensions[eigen];
normalizedVectors = Map[Normalize, eigen, {2}];

secondVectors = Take[normalizedVectors,All, {3}];
(*Change which eigenvectors to use here->{?}*)
(*eigenvalues are +-3/2 for {1,2} and +-1/2 for {3,4}*)

\[Psi]\[Dagger] = Map[Conjugate, secondVectors];
\[Psi] = Map[ConjugateTranspose, \[Psi]\[Dagger]];
Table[\[Psi]\[Dagger][[i]].\[Psi][[i]], {i, 1, dim[[1]]}];
Flatten[%, 2]; (*This is a big list of values, in a long vector form*)

\[CapitalLambda]x ={{0, (Sqrt[3]/2), 0, 0},
```

```
{(Sqrt[3]/2), 0, 1, 0}, {0, 1, 0, (Sqrt[3]/2)}, {0, 0, (Sqrt[3]/2), 0}};
\[CapitalLambda]x2 = \[CapitalLambda]x.\[CapitalLambda]x;

Lx =  Table[\[Psi]\[Dagger][[i]].\[CapitalLambda]x.\[Psi][[i]], {i,1,dim[[1]]}];
Lx2 = Table[\[Psi]\[Dagger][[i]].\[CapitalLambda]x2.\[Psi][[i]], {i,1, dim[[1]]}];

\[CapitalLambda]y ={{0, -I*(Sqrt[3]/2), 0, 0},
{I*(Sqrt[3]/2), 0, -I, 0}, {0, I, 0, -I*(Sqrt[3]/2)}, {0, 0,I*(Sqrt[3]/2), 0}};
\[CapitalLambda]y2 = \[CapitalLambda]y.\[CapitalLambda]y;

Ly = Table[\[Psi]\[Dagger][[i]].\[CapitalLambda]y.\[Psi][[i]], {i,1,dim[[1]]}];
Ly2 = Table[\[Psi]\[Dagger][[i]].\[CapitalLambda]y2.\[Psi][[i]], {i,1,dim[[1]]}];

\[CapitalDelta]Lx = Sqrt[Lx2 - Lx^2];
\[CapitalDelta]Ly = Sqrt[Ly2 - Ly^2];

LHS = Flatten[\[CapitalDelta]Lx*\[CapitalDelta]Ly, 2];
dir[theta_, phi_] := {Sin[theta]*Cos[phi], Sin[theta]*Sin[phi],Cos[theta]}
sphereValues = Flatten[Table[dir[\[Theta], \[Phi]], {\[Theta], 0.0, Pi, Pi/h},
{\[Phi], 0.0,2*Pi, 2*Pi/h}], 1];

ListSurfacePlot3D[Chop[sphereValues*LHS], MaxPlotPoints -> m]
```

The following code is for calculating the Robertson and Schrödinger uncertainties, for $J_x^{(3/2)}$ and $J_y^{(3/2)}$.

```
Clear["`*"]
h = 30; (*step size*)m = 25;(*plot points*)

M ={{3/2 Cos[\[Theta]],Sqrt[3]/2 Sin[\[Theta]]*E^(-I*\[Phi]), 0, 0},
{Sqrt[3]/2 Sin[\[Theta]]*E^(I*\[Phi]), 1/2 Cos[\[Theta]],Sin[\[Theta]]*E^(-I*\[Phi]), 0},
{0, Sin[\[Theta]]*E^(I*\[Phi]), -1/2*Cos[\[Theta]], Sqrt[3]/2 Sin[\[Theta]]*E^(-I*\[Phi])},
{0, 0, Sqrt[3]/2 Sin[\[Theta]]*E^(I*\[Phi]), -3/2 Cos[\[Theta]]}};

Flatten[Table[M, {\[Theta], 0.0, Pi, Pi/h}, {\[Phi], 0.0, 2*Pi, 2*Pi/h}], 1];
eigen = Chop[Map[Eigenvectors, %]];
dim = Dimensions[eigen];
normalizedVectors = Map[Normalize, eigen, {2}];
```

```
secondVectors = Take[normalizedVectors, All, {3}];
(*Change which eigenvectors to use here->{?}*)
(*eigenvalues are +-3/2 for {1,2} and +-1/2 for {3,4}*)

\[Psi]\[Dagger] = Map[Conjugate, secondVectors];
\[Psi] = Map[ConjugateTranspose, \[Psi]\[Dagger]];
Table[\[Psi]\[Dagger][[i]].\[Psi][[i]], {i, 1, dim[[1]]}];
Flatten[%, 2]; (*This is a big list of values, in a long vector form*)

\[CapitalLambda]x ={{0, (Sqrt[3]/2), 0, 0}, {(Sqrt[3]/2), 0, 1, 0},
{0, 1, 0, (Sqrt[3]/2)}, {0, 0, (Sqrt[3]/2), 0}};
Lx =  Table[\[Psi]\[Dagger][[i]].\[CapitalLambda]x.\[Psi][[i]], {i, 1,dim[[1]]}];

\[CapitalLambda]y ={{0, -I*(Sqrt[3]/2), 0,0},
 {I*(Sqrt[3]/2), 0, -I, 0}, {0, I, 0, -I*(Sqrt[3]/2)}, {0, 0,I*(Sqrt[3]/2), 0}};
Ly = Table[\[Psi]\[Dagger][[i]].\[CapitalLambda]y.\[Psi][[i]], {i, 1, dim[[1]]}];
\[CapitalLambda]x\[CapitalLambda]y = \[CapitalLambda]x.\[CapitalLambda]y;

LxLy = Table[\[Psi]\[Dagger][[i]].\[CapitalLambda]x\[CapitalLambda]y.\[Psi][[i]], {i, 1,dim[[1]]}];

\[CapitalLambda]y\[CapitalLambda]x = \[CapitalLambda]y.\[CapitalLambda]x;
LyLx = Table[\[Psi]\[Dagger][[i]].\[CapitalLambda]y\[CapitalLambda]x.\[Psi][[i]], {i, 1,dim[[1]]}];

Com = LxLy - LyLx;
ACom = LxLy + LyLx;

Robertson = Flatten[Sqrt[(1/(2*I)*Com)^2], 2];
Schrodinger = Flatten[Sqrt[(1/2*ACom - Lx*Ly)^2 + (1/(2*I)*Com)^2], 2];

dir[theta_, phi_] := {Sin[theta]*Cos[phi], Sin[theta]*Sin[phi],Cos[theta]}
sphereValues = Flatten[Table[dir[\[Theta], \[Phi]], {\[Theta], 0.0, Pi, Pi/h},
{\[Phi], 0.0,2*Pi, 2*Pi/h}], 1];

ListSurfacePlot3D[Chop[sphereValues*Robertson], MaxPlotPoints -> m]

ListSurfacePlot3D[Chop[sphereValues*Schrodinger], MaxPlotPoints -> m]
```

B.3 Code for $\mathbf{J}_r^{(2)}$

The following is the code for calculating $\sigma_{J_x^{(2)}}\sigma_{J_y^{(2)}}$.

```
Clear["`*"]
h = 30; (*step size*)m = 22;(*plot points*)

M ={{2 Cos[\[Theta]], Sin[\[Theta]] E^(-I*\[Phi]), 0, 0,0},
{Sin[\[Theta]] E^(I*\[Phi]), Cos[\[Theta]],Sqrt[6]/2*Sin[\[Theta]] E^(-I*\[Phi]), 0, 0},
{0,Sqrt[6]/2*Sin[\[Theta]] E^(I*\[Phi]), 0,Sqrt[6]/2*Sin[\[Theta]] E^(-I*\[Phi]), 0},
{0, 0,Sqrt[6]/2*Sin[\[Theta]] E^(I*\[Phi]), -Cos[\[Theta]],Sin[\[Theta]] E^(-I*\[Phi])},
{0, 0, 0,Sin[\[Theta]] E^(I*\[Phi]), -2 Cos[\[Theta]]}};

Flatten[Table[M, {\[Theta], 0.0, Pi, Pi/h}, {\[Phi], 0.0, 2*Pi, 2*Pi/h}], 1];
eigen = Chop[Map[Eigenvectors, %]];
dim = Dimensions[eigen];
normalizedVectors = Map[Normalize, eigen, {2}];

secondVectors = Take[normalizedVectors,All, {3}];
(*Change which eigenvectors to use here->{?}*)
(*eigenvalues are +-3/2 for {1,2} and +-1/2 for {3,4}*)

\[Psi]\[Dagger] = Map[Conjugate, secondVectors];
\[Psi] = Map[ConjugateTranspose, \[Psi]\[Dagger]];
Table[\[Psi]\[Dagger][[i]].\[Psi][[i]], {i, 1, dim[[1]]}];
Flatten[%, 2]; (*This is a big list of values, in a long vector form*)

\[CapitalLambda]x = {{0, 1, 0, 0, 0}, {1, 0, (Sqrt[6]/2),0, 0},
{0, (Sqrt[6]/2), 0, (Sqrt[6]/2), 0}, {0, 0, (Sqrt[6]/2), 0,1}, {0, 0, 0, 1, 0}};
\[CapitalLambda]x2 = \[CapitalLambda]x.\[CapitalLambda]x;

Lx =  Table[\[Psi]\[Dagger][[i]].\[CapitalLambda]x.\[Psi][[i]], {i, 1,dim[[1]]}];
Lx2 = Table[\[Psi]\[Dagger][[i]].\[CapitalLambda]x2.\[Psi][[i]], {i,1, dim[[1]]}];

\[CapitalLambda]y = {{0, -I, 0, 0, 0}, {I, 0, -I (Sqrt[6]/2), 0, 0},
{0, I (Sqrt[6]/2), 0, -I (Sqrt[6]/2),0}, {0, 0, I (Sqrt[6]/2), 0, -I}, {0, 0, 0, I, 0}};
\[CapitalLambda]y2 = \[CapitalLambda]y.\[CapitalLambda]y;

Ly = Table[\[Psi]\[Dagger][[i]].\[CapitalLambda]y.\[Psi][[i]], {i,1,dim[[1]]}];
```

```
Ly2 = Table[\[Psi]\[Dagger][[i]].\[CapitalLambda]y2.\[Psi][[i]], {i,1,dim[[1]]}];

\[CapitalDelta]Lx = Sqrt[Lx2 - Lx^2];
\[CapitalDelta]Ly = Sqrt[Ly2 - Ly^2];

LHS = Flatten[\[CapitalDelta]Lx*\[CapitalDelta]Ly, 2];
dir[theta_, phi_] := {Sin[theta]*Cos[phi], Sin[theta]*Sin[phi],Cos[theta]}
sphereValues = Flatten[Table[dir[\[Theta], \[Phi]], {\[Theta], 0.0, Pi, Pi/h},
{\[Phi], 0.0,2*Pi, 2*Pi/h}], 1];

ListSurfacePlot3D[Chop[sphereValues*LHS], MaxPlotPoints -> m]
```

The following code is for calculating the Robertson and Schrödinger uncertainties, for $J_x^{(2)}$ and $J_y^{(2)}$.

```
Clear["`*"]
h = 30; (*step size*)m = 25;(*plot points*)

M ={{2 Cos[\[Theta]], Sin[\[Theta]] E^(-I*\[Phi]), 0, 0,0},
{Sin[\[Theta]] E^(I*\[Phi]), Cos[\[Theta]],Sqrt[6]/2*Sin[\[Theta]] E^(-I*\[Phi]), 0, 0},
{0,Sqrt[6]/2*Sin[\[Theta]] E^(I*\[Phi]), 0,Sqrt[6]/2*Sin[\[Theta]] E^(-I*\[Phi]), 0},
{0, 0,Sqrt[6]/2*Sin[\[Theta]] E^(I*\[Phi]), -Cos[\[Theta]],Sin[\[Theta]] E^(-I*\[Phi])},
{0, 0, 0,Sin[\[Theta]] E^(I*\[Phi]), -2 Cos[\[Theta]]}};

Flatten[Table[M, {\[Theta], 0.0, Pi, Pi/h}, {\[Phi], 0.0, 2*Pi, 2*Pi/h}], 1];
eigen = Chop[Map[Eigenvectors, %]];
dim = Dimensions[eigen];
normalizedVectors = Map[Normalize, eigen, {2}];

secondVectors = Take[normalizedVectors, All, {3}];
 (*Change which eigenvectors to use here->{?}*)
(*eigenvalues are +-3/2 for {1,2} and +-1/2 for {3,4}*)

\[Psi]\[Dagger] = Map[Conjugate, secondVectors];
\[Psi] = Map[ConjugateTranspose, \[Psi]\[Dagger]];
Table[\[Psi]\[Dagger][[i]].\[Psi][[i]], {i, 1, dim[[1]]}];
Flatten[%, 2]; (*This is a big list of values, in a long vector form*)

\[CapitalLambda]x = {{0, 1, 0, 0, 0}, {1, 0, (Sqrt[6]/2),0, 0},
```

```
{0, (Sqrt[6]/2), 0, (Sqrt[6]/2), 0}, {0, 0, (Sqrt[6]/2), 0,1}, {0, 0, 0, 1, 0}};
Lx =  Table[\[Psi]\[Dagger][[i]].\[CapitalLambda]x.\[Psi][[i]], {i, 1,dim[[1]]}];

\[CapitalLambda]y ={{0, -I, 0, 0, 0}, {I, 0, -I (Sqrt[6]/2), 0, 0},
{0, I (Sqrt[6]/2), 0, -I (Sqrt[6]/2),0}, {0, 0, I (Sqrt[6]/2), 0, -I}, {0, 0, 0, I, 0}};
Ly = Table[\[Psi]\[Dagger][[i]].\[CapitalLambda]y.\[Psi][[i]], {i, 1, dim[[1]]}];

\[CapitalLambda]x\[CapitalLambda]y = \[CapitalLambda]x.\[CapitalLambda]y;
LxLy = Table[\[Psi]\[Dagger][[i]].\[CapitalLambda]x\[CapitalLambda]y.\[Psi][[i]], {i, 1,dim[[1]]}];

\[CapitalLambda]y\[CapitalLambda]x = \[CapitalLambda]y.\[CapitalLambda]x;
LyLx = Table[\[Psi]\[Dagger][[i]].\[CapitalLambda]y\[CapitalLambda]x.\[Psi][[i]], {i, 1,dim[[1]]}];

Com = LxLy - LyLx;
ACom = LxLy + LyLx;

Robertson = Flatten[Sqrt[(1/(2*I)*Com)^2], 2];
Schrodinger = Flatten[Sqrt[(1/2*ACom - Lx*Ly)^2 + (1/(2*I)*Com)^2], 2];

dir[theta_, phi_] := {Sin[theta]*Cos[phi], Sin[theta]*Sin[phi],Cos[theta]}
sphereValues = Flatten[Table[dir[\[Theta], \[Phi]], {\[Theta], 0.0, Pi, Pi/h},
{\[Phi], 0.0,2*Pi, 2*Pi/h}], 1];

ListSurfacePlot3D[Chop[sphereValues*Robertson], MaxPlotPoints -> m]

ListSurfacePlot3D[Chop[sphereValues*Schrodinger], MaxPlotPoints -> m]
```

Appendix C

Mathematica Code for Numerical Calculations of Fidelity via Operator Norms

The following code is for when the quantum gate U is the Hadmard gate. The code for when U is one of the two other U's is exactly the same except U and $U^\dagger$ are replaced with the particular U instead.

```
Clear["`*"]
c1 = 1/2;(*Eigenvalue*)h = 6.4;(*Step Size: Memory is exhausted at step size of 6.4*)
\[Sigma]x = {{0, 1}, {1,0}}; \[Sigma]y = {{0, -I}, {I, 0}}; \[Sigma]z = {{1, 0}, {0, -1}};
\[Sigma] = {\[Sigma]x, \[Sigma]y, \[Sigma]z};

u = {Sin[\[Theta]] Cos[\[Phi]], Sin[\[Theta]] Sin[\[Phi]], Cos[\[Theta]]};
l = {Sin[\[Omega]] Cos[\[Chi]],Sin[\[Omega]] Sin[\[Chi]], Cos[\[Omega]]};

Ls = c1*l.\[Sigma];
U = 1/Sqrt[2] {{1, 1}, {1, -1}}; U\[Dagger] = 1/Sqrt[2] {{1, 1}, {1, -1}};
Us = E^(I*\[Zeta]) (Cos[\[Xi]/2]*IdentityMatrix[2] + I*Sin[\[Xi]/2] (u.\[Sigma]));
Us\[Dagger] = E^(-I*\[Zeta]) (Cos[\[Xi]/2]*IdentityMatrix[2] - I*Sin[\[Xi]/2] (u.\[Sigma]));
```

```
Ddi = U\[Dagger].Ls.U - Us\[Dagger].Ls.Us;
Flatten[Chop[Table[Ls, {\[Theta], 0, Pi, Pi/h}, {\[Phi], 0, 2 Pi, 2 Pi/h},
{\[Omega], 0, Pi, Pi/h}, {\[Chi], 0, 2 Pi, 2 Pi/h}, {\[Xi], 0, Pi, Pi/h}, {\[Zeta], 0, 2 Pi, 2 Pi/h}]], 5];
dimLs = Dimensions[%];
Table[Eigenvalues[Transpose[%%[[i]]].%%[[i]]], {i, 1, dimLs[[1]]}];
LsV = Sqrt[Max[Re[%]]];(*Ls is 0.5*)

Flatten[Chop[Table[Ddi, {\[Theta], 0, Pi, Pi/h}, {\[Phi], 0, 2 Pi,2 Pi/h},
{\[Omega], 0, Pi, Pi/h}, {\[Chi], 0, 2 Pi,2 Pi/h}, {\[Xi], 0, Pi, Pi/h}, {\[Zeta], 0, 2 Pi, 2 Pi/h}]], 5];
dimDd = Dimensions[%];
Table[Eigenvalues[Transpose[%%[[i]]].%%[[i]]], {i, 1, dimDd[[1]]}];
DdV = Sqrt[ Max[Re[%]]] ;

Comi = -Us\[Dagger].Ls.Us.Ls + Ls.Us\[Dagger].Ls.Us;
Flatten[Chop[Table[Comi, {\[Theta], 0, Pi, Pi/h}, {\[Phi], 0, 2 Pi, 2 Pi/h},
{\[Omega], 0, Pi, Pi/h}, {\[Chi], 0, 2 Pi, 2 Pi/h}, {\[Xi], 0, Pi, Pi/h}, {\[Zeta], 0, 2 Pi, 2 Pi/h}]], 5];
dimCom = Dimensions[%];
Table[Eigenvalues[Transpose[%%[[i]]].%%[[i]]], {i, 1, dimCom[[1]]}];

Com = Sqrt[Max[Re[%]]];
AComi = U\[Dagger].Ls.U.Ls - Us\[Dagger].Ls.Us.Ls +Ls.U\[Dagger].Ls.U + Ls.Us\[Dagger].Ls.Us;
Flatten[Chop[Table[AComi, {\[Theta], 0, Pi, Pi/h}, {\[Phi], 0, 2 Pi, 2 Pi/h},
{\[Omega], 0, Pi, Pi/h}, {\[Chi], 0, 2 Pi, 2 Pi/h}, {\[Xi], 0, Pi, Pi/h}, {\[Zeta], 0, 2 Pi, 2 Pi/h}]], 5];
dimACom = Dimensions[%];
Table[Eigenvalues[Transpose[%%[[i]]].%%[[i]]], {i, 1, dimACom[[1]]}];

ACom = Sqrt[ Max[Re[%]]];

Rob = Sqrt[1 - (1/(4 c1^2)) ((1/(2) Com)^2)]
Schrod = Sqrt[ 1 - (1/(4 c1^2)) ((1/(2) Com)^2 + (1/2 ACom - DdV*LsV)^2)]
```

Index

angular momentum matrices, 61

Bloch sphere, 9, 18, 42

conservation law, 4, 8, 44, 45, 47
covariance, 14

density operator, 17, 18, 35, 50
deviation operator, 45–47

fidelity, 9, 42–45, 47, 49, 52, 59

Hawking, 2
Heisenberg, 2, 14
Heisenberg uncertainty principle, 2, 3, 13

incompatible observables, 46

orbital angular momentum, 4–7

Planck, 2
polarization, 18

Robertson uncertainty relation, 3, 4, 13, 14, 25, 30, 35, 38, 46, 59

Schrödinger uncertainty relation, 3, 4, 8, 14, 16, 19, 22, 25, 30, 35, 38, 44, 46, 47, 50, 59
Schwarz inequality, 15, 19, 22
spin, 4–7, 18, 25, 32, 33, 50, 63

trace, 17

Weyl, 3, 13, 22
Wigner-Araki-Yanase theorem, 44–46

Bibliography

[1] W. Heisenberg, "Über den anschaulichen Inhalt der quantentheoretischen Kinematik und Mechanik," Z. Phys. **43,** 172–198 (1927).

[2] H. P. Robertson, "The Uncertainty Principle," Phys. Rev. **34,** 163–64 (1929).

[3] E. Schrödinger, "Zum Heisenbergschen Unschärfeprinzip," Sitzungsber. Preuss. Akad. Wiss. Phys. Math. Kl. **14,** 296–303 (1930).

[4] N. J. Steiger and J.-F. S. Van Huele, "Quantifying Incompatibility: Ramifications of Extending Angular Momentum Uncertainty Relations," J. Utah Acad. Sci. **86,** 197–209 (2010).

[5] T. Karasawa, J. Gea-Banacloche, and M. Ozawa, "Gate fidelity of arbitrary single-qubit gates constrained by conservation laws," J. Phys. A **42,** 225303 (2009).

[6] W. Heisenberg, "Über die Grundprinzipien der Quantenmechanik," Forsch. Fortschr. **3,** 83 (1927).

[7] *Quantum Theory and Measurement*, 1st ed., J. A. Wheeler and W. H. Zurek, eds., (Princeton U.P., Princeton, N.J., 1983).

[8] A. Whitaker, *Einstein, Bohr and the Quantum Dilemma* (Cambridge U.P., Cambridge, UK, 2006).

[9] D. J. Griffiths, *Introduction to Quantum Mechanics*, 2nd ed. (Pearson, New Jersey, 2005).

[10] S. Hawking, *The Universe in a Nutshell* (Bantam, Princeton, N.J., 2002).

[11] M. Planck, "Ueber das Gesetz der Energieverteilung im Normalspectrum," Ann. Phys. **309,** 553–563 (1901).

[12] H. Weyl, *Gruppentheorie Und Quantenmechanik* (Hirzel, Leipzig, 1928).

[13] D. Lindley, *Uncertainty: Einstein, Heisenberg, Bohr, and the Struggle for the Soul of Science*, 1st ed. (Doubleday, New York, N.Y., 2007).

[14] W. C. Price, S. S. Chissick, and W. Heisenberg, *The Uncertainty Principle and Foundations of Quantum Mechanics: A Fifty Years Survey*, 1st ed. (Wiley, New York, N.Y., 1977).

[15] NASA/JPL-Caltech, "PIA12505: Probing Exoplanets From the Ground," http://photojournal.jpl.nasa.gov/catalog/PIA12505 (Accessed 8 April 2010).

[16] T. D. Ladd, F. Jelezko, R. Laflamme, Y. Nakamura, C. Monroe, and J. L. O'Brien, "Quantum computers," Nature **464,** 45–53 (2010).

[17] E. Knill, "Quantum computing with realistically noisy devices," Nature **434,** 39–44 (2005).

[18] M. Nielsen and I. Chuang, *Quantum Computation and Quantum Information* (Cambridge U.P., Cambridge, 2000).

[19] E. Merzbacher, *Quantum Mechanics*, 3rd ed. (Wiley, New York, 1998).

[20] A. Angelow, "Evolution of Schrödinger Uncertainty Relation in Quantum Mechanics," NeuroQuantology **7,** 325–331 (2009).

[21] K. F. Riley, M. P. Hobson, and S. J. Bence, *Mathematical Methods for Physics and Engineering*, 3rd ed. (Cambridge U.P., Cambridge, UK, 2006).

[22] M. B. Mensky, *Quantum Measurements and Decoherence: Models and Phenomenology* (Kluwer, Dordrecht, Netherlands, 2000).

[23] L. Ballentine, *Quantum Mechanics* (World Scientific, Singapore, 1998).

[24] A. Angelow and M. Batoni, "Translation with Annotation of the Original Paper of Erwin Schrödinger (1930) in English," Bulg. J. Phys. **26,** 193–203 (1999).

[25] E. P. Wigner, Z. Phys. **133,** 101 (1952).

[26] H. Araki and M. M. Yanase, "Measurement of Quantum Mechanical Operators," Phys. Rev. **120,** 622–626 (1960).

[27] M. Ozawa, "Conservative Quantum Computing," Phys. Rev. Lett. **89,** 057902 (2002).

[28] M. Ozawa, "Uncertainty Principle For Quantum Instruments and Computing," Int. J. Quant. Inf. **1,** 569–588 (2003).

[29] W. Dür, H.-J. Briegel, J. I. Cirac, and P. Zoller, "Quantum repeaters based on entanglement purification," Phys. Rev. A **59,** 169–181 (1999).

[30] E. Knill, R. Laflamme, and G. J. Milburn, "A scheme for efficient quantum computation with linear optics," Nature **409,** 46–52 (2001).

[31] R. L. Liboff, *Introductory Quantum Mechanics*, 4th ed. (Addison Wesley, San Francisco, 2003).